NASA
Technical
Paper
2337

June 1984

NASA-TP-2337 19840018330

A Stochastic Model for Photon Noise Induced by Charged Particles in Multiplier Phototubes of the Space Telescope Fine Guidance Sensors

Leonard W. Howell
and Hans F. Kennel

NASA

NASA
Technical
Paper
2337

1984

A Stochastic Model for Photon Noise Induced by Charged Particles in Multiplier Phototubes of the Space Telescope Fine Guidance Sensors

Leonard W. Howell
and Hans F. Kennel

George C. Marshall Space Flight Center
Marshall Space Flight Center, Alabama

NASA
National Aeronautics
and Space Administration

**Scientific and Technical
Information Branch**

ACKNOWLEDGMENTS

We hereby express our appreciation to Drs. Good,[1] Parnell,[2] and Teich[3] for their expert assistance in the preparation of this paper.

1. Irving John Good, University Distinguished Professor of Statistics, Virginia Polytechnic Institute and State University, Blacksburg, VA 24061.

2. Thomas A. Parnell, Chief, High Energy Physics Branch, Space Science Laboratory, Marshall Space Flight Center, Huntsville, AL 35812.

3. Malvin C. Teich, Professor of Electrical Engineering, Columbia University, New York, NY 10027.

TABLE OF CONTENTS

LIST OF ILLUSTRATIONS

LIST OF ILLUSTRATIONS (Concluded)

LIST OF TABLES

TECHNICAL PAPER

A STOCHASTIC MODEL FOR PHOTON NOISE INDUCED BY CHARGED PARTICLES IN MULTIPLIER PHOTOTUBES OF THE SPACE TELESCOPE FINE GUIDANCE SENSORS

I. INTRODUCTION

A. General

The pioneering observatory Space Telescope (ST) is scheduled for operation in Earth-orbit beginning in mid-1986.

For the ST to perform its mission, very accurate line-of-sight stability must be maintained for periods up to 10 hr. To maintain this stability, the attitude information is provided by two on-board Fine Guidance Sensors (FGS) (a third FGSS is either on stand-by or it is performing astrometry). The FGS track guide-stars through the main telescope. Each FGS has two multiplier phototube (PMT) pairs (Fig. 1), one pair for each axis. Pointing stability is maintained by detecting deviations from the viewing object using the difference in guide star photon counts in one or more of the PMT pairs. These photons are detected by a photocathode on the inner side of the PMT glass window. Because of ST exposure to charged particles in its space environment, concern arose over the possibility that incoming particles would strike the glass window, creating a flash of Cerenkov radiation[1] and secondary fluorescence as the particle bores its way through the glass.

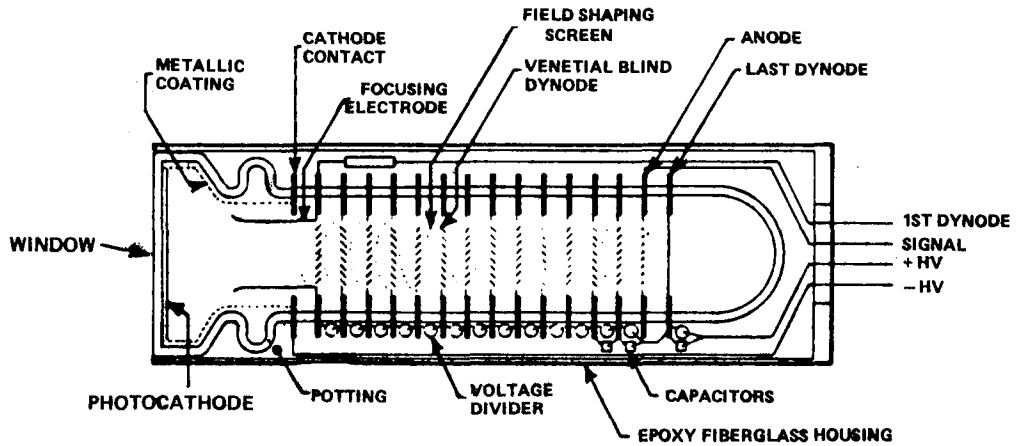

Figure 1. Multiplier phototube cross section.

1. Cerenkov radiation. The radiation from a charged particle whose velocity is greater than the phase velocity that an electromagnetic wave would have if it were propagating in the medium. The particle will continue to lose energy by radiation until its velocity is less than this phase velocity. This phenomenon is analogous to the generation of a shock wave when an object is traveling faster than the velocity of sound in the medium. A bow wave is set up that radiates energy into the medium and slows down the object. The angle that the cone of radiation makes with the direction of motion of the particle can be used to measure the velocity of the particle. Named after the Russian physicist Pavel A. Cerenkov, born 1904; Nobel prize 1958 [1].

Because the photocathode cannot distinguish the source of the photons, those photons generated by the charged particle (which then strike the photocathode) will cause an increased photon count in the struck PMT. This would appear as an increase in apparent star brightness and would produce a large differential count between pairs of PMTs resulting in a ST attitude disturbance, possibly large enough to lose "lock" on the desired guide star. The Cerenkov flash is very short lived (less than 70 ps) and causes only one photon count with an associated pulse amplitude proportional to the number of Cerenkov photons striking the photocathode because the time resolution of the PMT pulse amplitude discriminator (PAD) is approximately 75 ns. However, the duration of the fluorescence follows an exponential distribution, with a time constant of several 100 μs and every fluorescence photon is counted. This gave rise to the idea to detect the Cerenkov flash by an additional much higher PAD threshold and then blank the photon count for the next millisecond, eliminating the effect of the fluorescence photons. While others began to study the problem from an experimental point of view, we decided to use a simulation to derive the bivariate probability distribution for the number of Cerenkov counts and for the number of fluorescence counts registered by the photocathode for a single charged particle strike.

Because of the complexity of the physical setting and apparent random behavior of particle strikes, it was decided that a stochastic model for photon noise induced by charged particles be developed based on a computer simulation of the physical scenario. The resultant bivariate distribution of Cerenkov radiation and fluorescence would show the relationship between these two and determine whether the Cerenkov flash can be used to give reliable warning of the subsequent fluorescence. Secondly, these results may then be introduced into the ST attitude-control model to determine the effects of charged particles on ST pointing accuracy and to suggest possible remedies if required.

A comparison of the model's predictions with experimental results is also discussed, as well as a sensitivity study of some of the model's parameters.

B. Pointing Capability

The ST has three sources of information for its orientation: the Rate Gyroscopes, the Star Trackers, and the Fine Guidance Sensors. Since the primary goal is the prompt and accurate acquisition of preselected guide stars, all three sources of information are used when ST is pointed to a new object. The slewing rate is determined by reaction wheels and is specified to allow movement to objects 90 deg away in no more than 20 min, including angular acceleration and deceleration, with the reference frame provided by the Rate Gyroscopes. The Star trackers then use bright stars to determine the pointing to an accuracy of a few arc minutes, which is sufficient to place the guide stars in the field of the Fine Guidance System. Following an acquisition procedure to select the correct guide star, the guide star images are put through a 3 arc sec x 3 arc sec aperture and fed to an interferometric device which gives (through the use of a pair of PMTs per axis), the fine error signal that results in the overall guiding stability of 0.007 arc sec rms. The positioning of the Fine Guidance Sensors can be set to an accuracy of 0.001 arc sec.

C. Charged Particle[2] Environment

The nominal orbit for the ST is at an inclination of 28.8 deg and an altitude of 590 km (320 n.mi.). For this orbit, radiation-sensitive equipment will be subjected to a substantial flux of high energy charged particles and their induced secondary particle showers.

2. In this report, the term charged particle will apply to both cosmic ray nuclei and those particles trapped in the Van Allen Belt by the Earth's magnetic field.

There are three possible sources of radiation that can degrade the ST pointing performance: geomagnetically trapped electrons, protons, alpha particles (helium nuclei), and heavier nuclei, solar event protons, and galactic cosmic ray particles. Because the Earth's magnetic field at 30 deg latitude will eliminate protons below 4 BeV, solar flare protons should not be important. The dose rate of charged particles will be reduced by the geomagnetic field and the vehicle structure will shield against electrons. According to Stassinopoulos [2], the dose rate caused by particles for the nominal orbit should be about 0.7 rads/day (a rad is the deposition of 100 ergs of energy per gram of material receiving the dose).

When a relativistic charged particle passes through the multiplier phototube window, its speed is greater than that of light in the glass. This produces a cascade of conically directed photons, the resultant flash of Cerenkov radiation lasting less than 70 ps. Because the time resolution of the PMT electronics is 75 ns, the Cerenkov radiation is registered only as a single pulse of amplitude proportional to the number of Cerenkov photons striking the photocathode. During the next several hundred μs, fluorescence photons are emitted and those which strike the photocathode are individually registered as photon noise.

Since the photocathode is incapable of distinguishing between these photons and the incoming guide star photons, the biased 25 ms (millisecond) interval (cycle length of ST computer) count will be interpreted by the ST guidance system as an attitude offset from the guide star which will result in pointing disturbances.

D. Modeling Approach

The rate at which charged particles would strike the PMT window had been estimated from satellite data by others. Hence, it is sufficient to determine the resultant radiation effects of each strike. Consequently, the distribution of Cerenkov radiation and fluorescence is to be simulated from the physical scenario, conditional on having a charged particle strike the PMT window. Given that such a charged particle had struck the PMT window, its entry point was simulated by assuming that the likelihood of it striking the top, side wall, or bottom, would be proportional to that region's surface area, where, for geometrical convenience, the PMT window was idealized as a right circular cylinder. The outer window surface was considered the "top" and the inner surface the "bottom". The surface of entry was chosen by Monte Carlo methods and then a uniformly randomly distributed point on that surface was designated as the entry point.

Because direction of entry was assumed to have no preference, a uniformly distributed random point was selected on the surface of a hemisphere imagined to be placed over the entry point. The two points were then connected, giving the direction cosines of the particle's path as it enters the PMT window. The particle was followed to its exit point and the path length determined. Instantaneously Cerenkov photons are emitted, their number being a random variable assumed to follow a Poisson distribution with a mean proportional to the particle's path length through the glass and origin of departure of the individual photons being uniformly randomly distributed along the path. The direction of travel was randomly selected down the surface of a cone whose half-angle is determined by the particle's kinetic energy, with apex at the photon departure point and base towards the charged particle's exit. The distribution of the kinetic energy of charged particles trapped in the Van Allen Belt would also be estimated from available satellite data for the ST orbit, while a literature search revealed that the cosmic ray energy distribution followed a power law [3,4].

The path of each of these photons was then followed to determine its point of contact with the cylinder's interior surface. Those which were intercepted by the photocathode on the bottom left the system and contributed to the pulse amplitude of the Cerenkov radiation. Photons striking other regions

of the cylinder's surface either passed through the cylinder's surface and left the system or were reflected back into the cylinder depending on the angle of incidence. Reflected photons eventually would leave the system through either the photocathode or cylinder walls, or fall into trapped orbits within the cylinder and thus would not contribute to the FGS photon count.

II. MATHEMATICAL MODEL

NASA scientists had estimated that the probability of more than one cosmic ray strike in a 25 ms interval (the basic computational cycle of the ST computer) would be negligible.

Thus, this model is concerned with simulating the discrete bivariate distribution for the number of photons striking the photocathode from the Cerenkov radiation and the secondary fluorescence, respectively, given the event of a single charged particle having struck the PMT window.

The PMT window was idealized as a right circular cylinder with radius R and height H (Fig. 2). The effective photocathode was represented as a disk of radius r on the inner (bottom) side of the PMT window. Since every surface element of the PMT glass window is exposed to 2π steradians of space, it was assumed that the probability of a hit on any one of the cylinder's distinct surfaces (top, bottom, or side) was proportional to the surface's area. These areas are

$A_{tb} = \pi R^2$ top or bottom area

$A_{sd} = 2\pi H\ R$ side area

$A_{tot} = 2\pi R\ (R + H)$ total area

with R being the glass window radius, and H the glass window height. (See Appendix F for values of model parameters; Fig. 2 not drawn to scale.)

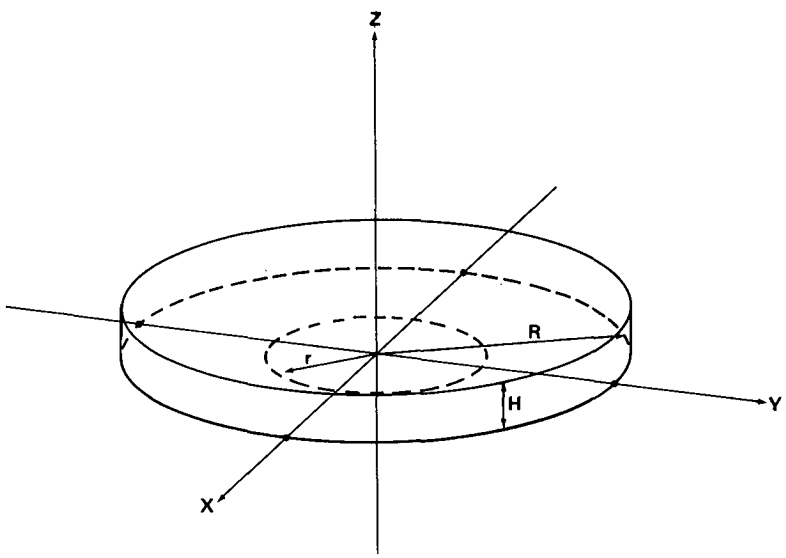

Figure 2. PMT window geometry.

The probabilities are then:

$$P_{tb} = A_{tb}/A_{tot} = R/(R + H) \tag{1}$$

$$P_{sd} = A_{sd}/A_{tot} = H/(R + H) \quad . \tag{2}$$

The direction cosines, selected such that the direction of the particle's path is uniformly distributed over 4π steradian, are given by[3]

$$[d_1, d_2, d_3]^T = [\cos\phi \cos\theta, \cos\phi \sin\theta, \sin\theta]^T \tag{3}$$

where

$\theta = \sin^{-1} [2(U_1 - 0.5)]$ elevation angle

$\phi = 2\pi U_2$ azimuth angle,

and the Us are different random numbers uniformly distributed between zero and one.

A decision is now made, whether the top/bottom, or side was hit:

$$U \begin{cases} < P_{tb} & \text{yields a top/bottom hit} \\ \geqslant P_{tb} & \text{results in a side hit.} \end{cases}$$

A. Top/Bottom Hit Entry

The coordinates of the top/bottom entry point are determined by

$$\begin{aligned} x &= R\,U \quad , \\ y &= R\,U \quad , \end{aligned} \tag{4}$$

(the Us are different uniform random numbers) and

3. See Appendices A, B, and C for the proof.

$$z = \begin{cases} H & \text{for } d_3 < 0 \\ \\ 0 & \text{for } d_3 \geqslant 0 \end{cases} .$$

The requirement that points (x,y) be uniformly distributed over a disk of radius R is met by first generating points uniformly distributed over the first quadrant of edge R and then rejecting those which lie outside the circle of radius R. (Because of symmetry, only one quadrant is necessary. For graphical purposes, the quadrants were later randomly indexed.)

B. Exit for Top/Bottom Entry

The change in position from entry point to exit point is first calculated as if the top or bottom of the window were an infinite plane. Thus,

$$\begin{bmatrix} \Delta x \\ \Delta y \\ \Delta z \end{bmatrix} = \begin{bmatrix} d_1 \\ d_2 \\ d_3 \end{bmatrix} [H\ I(d_3) - z]/d_3 \tag{5}$$

where I is the indicator function defined by

$$I(d_3) = \begin{cases} 1 & \text{for } d_3 \geqslant 0 \\ \\ 0 & \text{for } d_3 < 0 \end{cases} .$$

For top or bottom entries, z is either H or 0, but the same equation can be used for starting points after reflections, where z can be between 0 and H.

Notationally, any time a path or partial path is started at the window surface, the coordinates of its position are labeled as (x,y,z). Path endpoints are labeled (u,v,w). Ending can occur as an exit from the window, or with reflection, as the start of the next partial path.

In order to determine the exit point, the change in position is added to the entry point coordinates:

$$\begin{bmatrix} u \\ v \\ w \end{bmatrix} = \begin{bmatrix} x \\ y \\ z \end{bmatrix} + SC \begin{bmatrix} \Delta x \\ \Delta y \\ \Delta z \end{bmatrix} \tag{6}$$

A check is now made, whether this exit point (u,v,w) is within the window radius (scaling constant SC=1). If not, SC is reduced so that this condition is met by

$$SC = (b + \sqrt{b^2 + a(R^2 - x^2 - y^2)})/a \tag{7}$$

where

$$a = (\Delta x)^2 + (\Delta y)^2$$

and

$$b = -(x\Delta x + y\Delta y) \quad .$$

C. Side Hit Entry

Since the window is symmetric, the only relevant parameter for a side hit is the height z above the bottom of the window (z=0) and it is determined to be uniformly distributed as

$$z = H\,U \quad . \tag{8}$$

The other coordinates are arbitrarily fixed at

$$x = 0 \qquad \text{and} \qquad y = -R \quad .$$

However, for graphical purposes, we then rotate side entries through a uniformly distributed angle between 0 and 2π radians about the z-axis.

As previously discussed, direction cosines of the charged particle's path could be generated by connecting its entry point to a point uniformly distributed over the surface of a hemisphere centered over the entry point. However, mathematically, we found it more convenient to generate points distributed over the surface of a sphere and use the sign of the third direction cosine (d_3) to distinguish top and bottom particle strikes [equation (4)]. We set $d_2 = |d_2|$ in order to direct side hits always into the window.

D. Exit for Side Hit Entry

The unscaled exit position is

$$u = 2R\,d_1\,d_2/(1 - d_3^2)$$

$$v = (ud_2/d_1) - R \tag{9}$$

$$w = z + \Delta z \quad ,$$

where

$$\Delta z = u\, d_3/d_1 \quad .$$

To make sure that the path is physically possible, the following scaling checks have to be made

1) No top scaling is necessary if $\Delta z \leqslant (H - z)$

2) No bottom scaling is necessary if $-z \leqslant \Delta z$.

For top scaling we get

$$\begin{aligned} SC &= (H - z)/\Delta z \\ u &= SC\ u \\ v &= SC(v + R) - R \\ w &= H \quad . \end{aligned} \tag{10}$$

For bottom scaling we use

$$\begin{aligned} SC &= -z/\Delta z \\ u &= SC\ u \\ v &= SC\ (v + R) - R \\ w &= 0 \quad . \end{aligned} \tag{11}$$

E. Length Determination

Given the particle's entry and exit points, the path length

$$L = \sqrt{(x - u)^2 + (y - v)^2 + (z - w)^2} \tag{12}$$

is needed to determine the average number of Cerenkov and fluorescence photons.

F. Charged Particle Energy and Relative Speed

We distinguish two types of charged particles according to their energy distribution: Cosmic ray nuclei and charged particles trapped in the Earth's radiation belts. A power law (proportional to $E^{-\gamma}$) for the cosmic-ray energy spectrum is assumed, with the values of γ appearing in Table 1, where Z is the charge number or atomic number [3,4].

TABLE 1. CHARGED PARTICLE SPECTRAL INDICES, REST MASSES AND RELATIVE ABUNDANCES

Z	Particle	Index	Mass (kg)	Relative Abundance Above 1 GeV/Nucleon $(m^2 \cdot sr \cdot s)^{-1}$
1	Proton	2.70	1.67E-27	700
2	Alpha particle	2.70	6.6E-27	140
3	Lithium	3.35	11.5E-27	0.2
4	Beryllium	3.35	15.0E-27	0.2
5	Boron	3.35	18.0E-27	1.5
6	Carbon	2.76	20.0E-27	4.9
7	Nitrogen	3.07	23.0E-27	1.4
8	Oxygen	2.67	26.7E-27	4.5
9	Fluorine	3.01	31.7E-27	.18
10	Neon	2.88	33.1E-27	.73
11	Sodium	3.14	38.4E-27	.21
12	Magnesium	2.60	40.6E-27	.70
13	Aluminum	2.52	45.1E-27	.11
14	Silicon	2.63	46.9E-27	.53
.				
.				
.				
26	Iron	2.45	93.3E-27	.08

Thus, the following family of probability density functions for cosmic-ray energies per nucleon are obtained:

$$f(E) = (\gamma-1)\, E^{-\gamma} \quad , \tag{13}$$

where $1 \leqslant E < \infty$ (BeV), which leads to

$$E = U^{1/1-\gamma} \quad ,$$

as the desired random number generator. Because of the glass medium, nuclear interactions do not occur with significant frequency [5]. Thus, the more complicated electromagnetic cascade process referred to as the "soft component" of cosmic rays by Janossy [6], in which photons give rise to energetic electrons which in turn give rise to photons, is not modeled. The electromagnetic cascade process eventually comes to an end because of the loss of energy by ionization.

For protons trapped in the radiation belts, the flux differential for the ST orbit is shown in Figure 3 [7]. Because these protons are of much lower energy than the cosmic ray protons, the effect of shielding must be considered. The effective shielding for the ST was taken to be 7 mm of aluminum corresponding to the curve labeled by X=20 in Figure 3. A log-normal probability density function was found to be adequate, as suggested by References 8 and 9. It is of the form

$$f(E) = \frac{1}{E\sqrt{2\pi\,\sigma^2}}\; e^{-\frac{1}{2\sigma^2}(\ln E - \mu)^2} \tag{14}$$

where

$$0 < E < \infty \quad .$$

The desired log-normal generator for Van Allen belt proton and alpha particle energy per nucleon is:

$$E = e^{\mu + \sigma x} \quad , \tag{15}$$

where x is a standard normal random number and $\mu = 4.7$ and $\sigma = 1$.

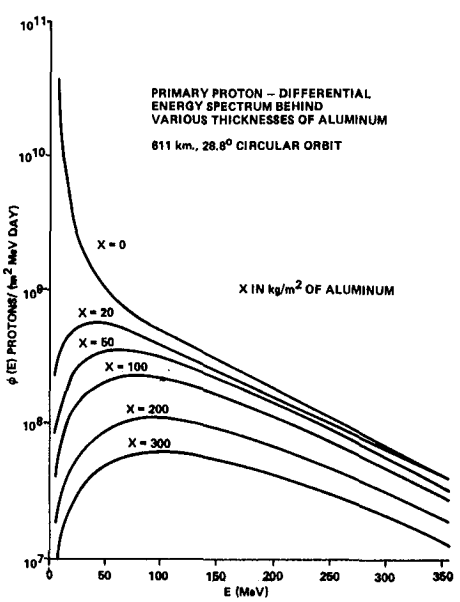

Figure 3. Average trapped proton flux differential with respect to energy at the center of a spherical aluminum shell of the given shield thicknesses for the ST orbit.

Thus, when modeling charged particle strikes in the Earth's radiation belts, equation (15) is used to simulate the particle's energy and equation (13) is used for cosmic ray nuclei strikes. Energies are then multiplied by K_{JFBEV} in order to convert to the SI system of units, where K_{JFBEV} = 1.60219E-10 is the conversion factor from billion electronvolts to Joules. The charged particle's speed relative to the speed of light c = 2.99792458E8 m/s can now be determined by

$$\beta = v/c = \sqrt{1 - 1/(1 + E/m_o\, c^2)} \tag{16}$$

where the primary charged particle's rest mass m_o is obtained from Table 1.

G. Number of Induced Photons

The Poisson mean for the number of induced Cerenkov photons is [10]

$$N_{CR} = (2\pi Z^2/k)\ [1 - 1/(\beta N_G)^2]\ F(\lambda)\ L \tag{17}$$

where Z is the charge number of the particle (atomic number); $k = (4\pi/\mu_0)\, e^2/hc \cong 137$ is the dimensionless fine structure constant, μ_o is the permeability coefficient, and h is Plank's constant, N_G = 1.49 is the refractive index of 7056 Pyrex glass; and L is the path length (mm) computed by equation (12). The factor F is a function of the wavelength of light and is given by F(λ) = 244 for 7056 Pyrex glass which was derived as follows [equation (2) of Reference 10]:

$$F(\lambda) = 1/\lambda_1 - 1/\lambda_2$$

for constant quantum efficiency. For varying efficiency e(λ), F(λ) is expressed as the integral

$$F(\lambda) = -0.5 \int_{\lambda_1}^{\lambda_2} [e(\lambda)/\lambda^2]\ d\lambda \quad . \tag{18}$$

Figure 4 shows the efficiency of 7056 Pyrex glass as a function of the wavelength [11]. Equation (18) was numerically evaluated from λ_1 = 350 nm to λ_2 = 800 nm, resulting in

$$F(\lambda) = 0.000\ 244\ 1/nm = 244\ mm^{-1} \quad .$$

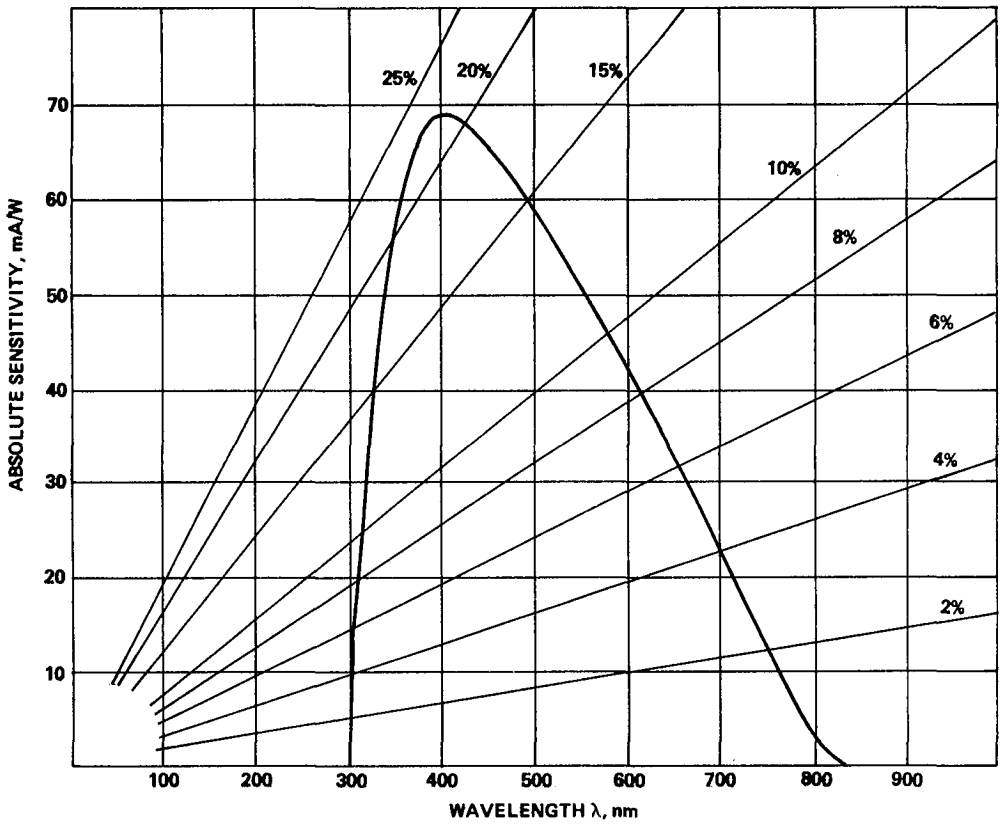

Figure 4. Radiant energy spectral coverage

The number of resultant photons comprising the fluorescence was assumed to follow a Poisson distribution with mean [12]

$$N_{FL} = K_{FL}\, L\, (dE/dx) \tag{19}$$

where

K_{FL} = 16 for 4π steradian , [13]

and dE/dx is determined by the restricted energy loss distribution (Appendix D).

Hence, the simulated number of induced photons for both the Cerenkov pulse amplitude height and secondary fluorescence is determined by the inverse cumulative distribution method described in Appendix B using the Poisson cumulative distribution function with the above means of N_{CR} and N_{FL}, respectively.

The simulated number of Cerenkov photons n_{CR} and fluorescence photons n_{FL} are then modeled as being uniformly randomly distributed along the charged particle's path. Their coordinates are determined by

$$(x_i,y_i,z_i) = (x,y,z) + (\Delta x,\Delta y,\Delta z)\ U_i \quad , \quad i = 1, \ldots, n_{CR}$$

for Cerenkov photons and

$$(x_i,y_i,z_i) = (x,y,z) + (\Delta x,\Delta y,\Delta z)\ U_i \quad , \quad i = 1, \ldots, n_{FL}$$

for fluorescence, where the U's are uniformly distributed random numbers and Δx, Δy, and Δz are the components of the pathlength L.

For Cerenkov radiation, the angle that the cone of luminescence makes with the direction of motion of the charged particle is determined by References 10 and 12 to be

$$\theta = \cos^{-1}(1/\beta N_G) \tag{20}$$

where β is determined from equation (16). The direction of departure of each of the n_{CR} photons will make an angle θ with the charged particle's path. The three-dimensional effect of the luminescent cone is simulated by rotating each photon's path through a random angle uniformly distributed over $(0,2\pi)$ using the Euler transformation

$$\begin{bmatrix} d_1 \\ d_2 \\ d_3 \end{bmatrix} = \begin{bmatrix} \cos\alpha_3 & -\sin\alpha_3 & 0 \\ \sin\alpha_3 & \cos\alpha_3 & 0 \\ 0 & 0 & 1 \end{bmatrix} \begin{bmatrix} \cos\alpha_2 & 0 & \sin\alpha_2 \\ 0 & 1 & 0 \\ -\sin\alpha_2 & 0 & \cos\alpha_2 \end{bmatrix} \begin{bmatrix} \cos\alpha_4 & \sin\alpha_4 & 0 \\ -\sin\alpha_4 & \cos\alpha_4 & 0 \\ 0 & 0 & 1 \end{bmatrix} \begin{bmatrix} 0 \\ \sin\alpha_1 \\ \cos\alpha_1 \end{bmatrix} \tag{21}$$

with

$$\alpha_1 = \cos^{-1}(1/\beta N_G)$$

$$\alpha_2 = \cos^{-1}(d_3)$$

$$\alpha_3 = \tan^{-1}(d_1/d_2)$$

$$\alpha_4 = 2\pi U \quad \text{(U is a uniform random number)} \quad .$$

Fluorescence photons are emitted uniformly in all directions. Consequently, direction cosines are generated for each of the n_{FL} photon paths by generating points uniformly distributed over the surface of a sphere and connecting each to the photon's departure point.

H. Total Reflection

The intensity of the reflected light R is [14]

$$R_{\perp} = \left(\frac{N_i \cos \theta_i - N_t \cos \theta_t}{N_i \cos \theta_i + N_t \cos \theta_t} \right)^2 \tag{22}$$

and

$$R_{\parallel} = \left(\frac{N_t \cos \theta_i - N_i \cos \theta_t}{N_i \cos \theta_t + N_t \cos \theta_i} \right)^2$$

where the intensity of the incident light is unity for perpendicularly polarized light ($\perp$) with respect to the plane of incidence as well as for the parallel polarized beam ($\parallel$) at the interface from a denser optical medium N_i to a less dense N_t and θ_i is the angle of incidence, θ_t the angle of transmission, both with respect to the interface normal. Figure 5 shows $R_{\perp}$ and $R_{\parallel}$ as a function of θ using $N_i = N_G = 1.49$ and $N_t = 1$. From an angle of 42.4 deg to 90 deg total reflection is obtained. Also shown in Figure 5 is the average

$$R = (R_{\perp} + R_{\parallel})/2 \tag{23}$$

which is used in the model under the assumption that the light is not necessarily polarized. The general geometry of reflection is shown in Figure 6. Because individual photons in the model are dealt with, R is interpreted to be the probability of being reflected. If a standard uniform random number is greater than R, the photon is lost through transmission. Otherwise it is reflected and then traced to its next point of contact with the surface of the PMT window. Note that for $\theta_i \geq \sin^{-1} (1/N_G) = 42.4$ deg, the photon will always be reflected.

Assuming a uniform distribution over a hemisphere, a cap with a cone angle of $\theta = 42.3$ deg represents only 26 percent of the hemisphere's surface area. Hence, 74 percent of the photons are totally reflected. In the modeling process, whenever the direction cosine of a photon measured with respect to the surface normal is

$$d_3 \leq d_{min} = \sqrt{1 - (1/N_G)^2} \quad , \tag{24}$$

total reflection is obtained.

If there is a top or bottom reflection, it is modeled by setting

$$d_3 = -d_3 \quad . \tag{25}$$

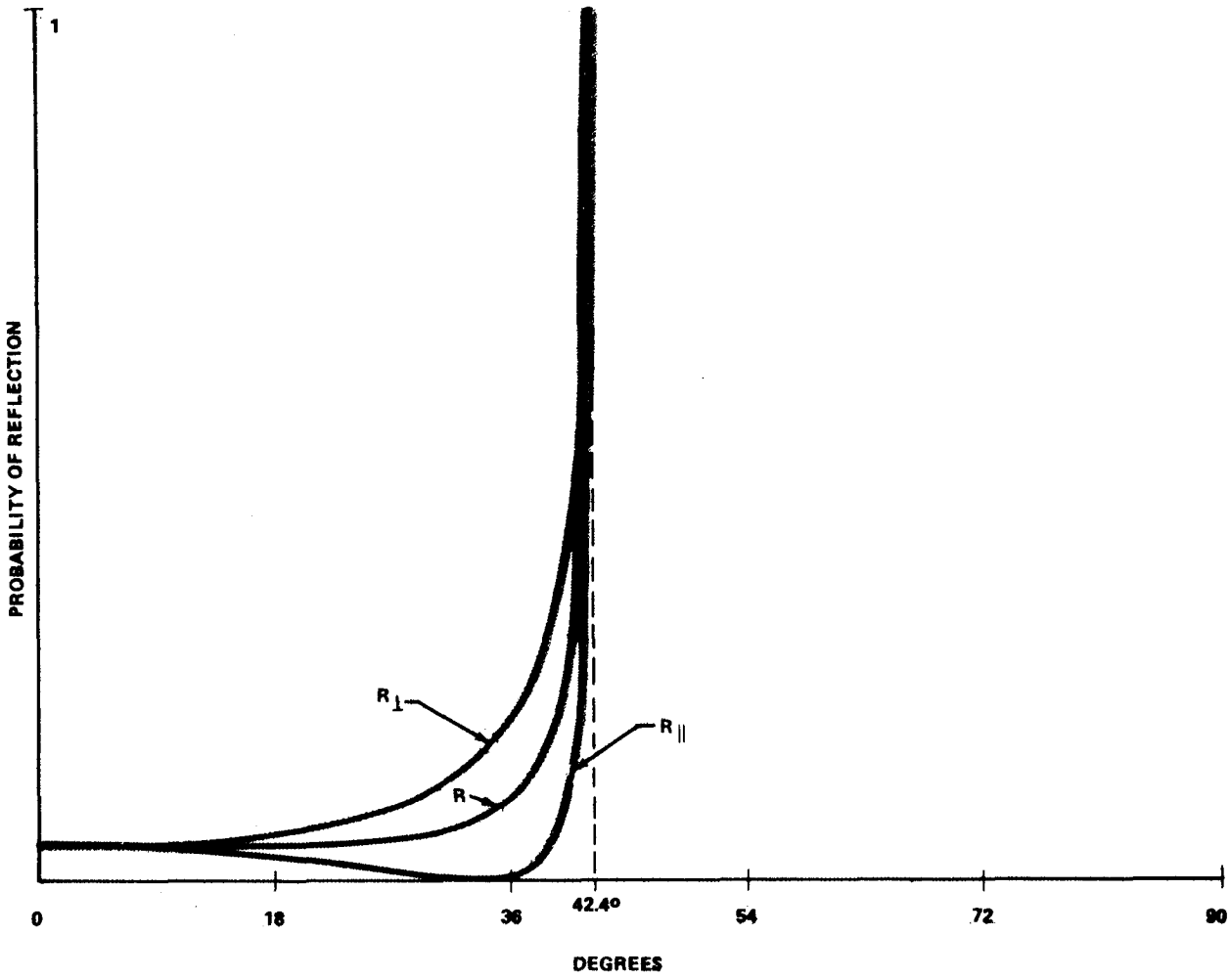

Figure 5. Intensity of reflected light.

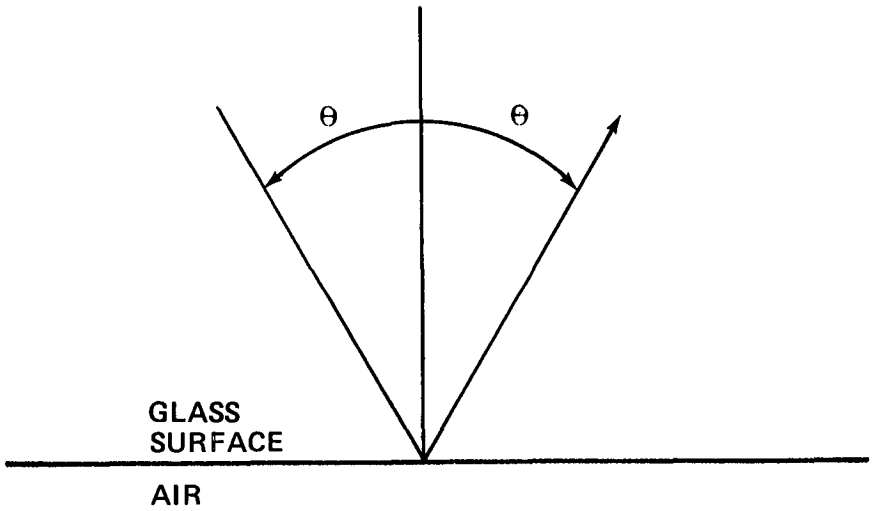

Figure 6. Geometry of reflection.

For a side reflection d_1 and d_2 are first transformed into components perpendicular and tangential to the side by

$$\begin{bmatrix} d_1' \\ d_2' \end{bmatrix} = \begin{bmatrix} \cos\alpha & \sin\alpha \\ -\sin\alpha & \cos\alpha \end{bmatrix} \begin{bmatrix} d_1 \\ d_2 \end{bmatrix} \tag{26}$$

with

$$\alpha = \tan^{-1}(u/v) \quad .$$

The perpendicular component is then used for the total reflection comparison

$$d_1' \leqslant d_{min} \quad .$$

If there is a total reflection it is achieved by reversing the sign of d_1' and then transforming back to the unprimed system as follows:

$$\begin{bmatrix} d_1 \\ d_2 \end{bmatrix} = \begin{bmatrix} \cos\alpha & -\sin\alpha \\ \sin\alpha & \cos\alpha \end{bmatrix} \begin{bmatrix} -d_1' \\ d_2' \end{bmatrix} \tag{27}$$

Considering the endpoint as the startpoint of a new partial path, the calculations are repeated until one of two conditions occurs.

1) The photon strikes the photocathode, liberates a photoelectron and the photon is absorbed. The photoelectron is counted if it strikes the effective photocathode area and a tally is kept.

2) The photon strikes the sides at such an angle that it could never strike the photocathode, but would continue to be reflected indefinitely. The photon is ignored as soon as this condition is recognized. Given an effective photocathode radius of r and a window radius of R, the photocathode cannot be struck if (Fig. 7)

$$|d_2'|/d_1' > r / \sqrt{R^2 - r^2} \tag{28}$$

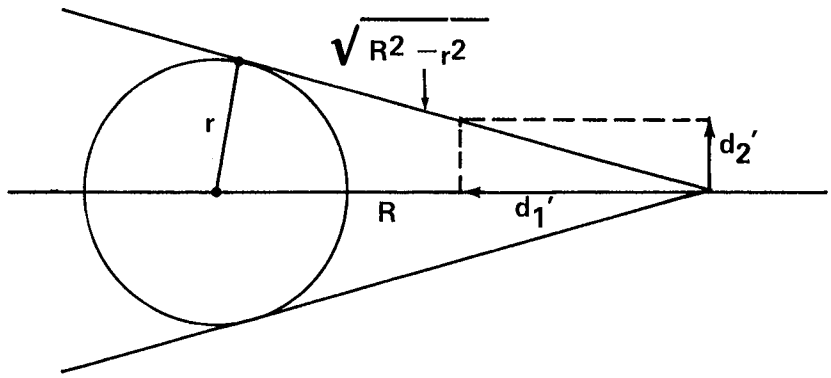

Figure 7. Geometry of rejection.

I. Modeling of the PMT Window Bottom

When the PMT is manufactured, the photocathode material is sputtered uniformly over the bottom of the PMT window. The photocathode radius of 1.5 mm used in the model represents the effective area of the PMT electronics. Thus, all photons which strike the bottom of the window and are transmitted through liberate an electron from the photocathode material. Electrons produced in the effective area contribute to the photon count, while those outside this region make no contribution. Photons which liberate electrons are considered to be incapable of later producing another electron and are thus eliminated from the simulation after electron production.

J. Photon Sink

The 1 mm thick wall of the PMT which connects the window with the rest of the tube acts as a photon sink in that those photons which go down the walls are modeled as escaping from the system.

K. Photon Absorption

The intensity of light through 1.83 m of glass is reduced by 50 percent. Thus, the probability of a photon traversing through L mm of glass is

$$P = e^{-kL} \qquad 0 \leqslant L < \infty \tag{29}$$

and

$$P \cong 1 - kL \text{ for small } L \ (0 \leqslant L \leqslant 19 \text{ mm}) \quad ,$$

where $k = 0.000379 \text{ mm}^{-1}$.

L. Photon Scattering

Scattering of internal reflections was investigated, but was found to be negligible and was consequently ignored in the simulation.

III. RESULTS

Because of ST's expected exposure to charged particles in its space environment, it is believed that the ST's pointing capabilities would be degraded. This had been recognized as inevitable during the time in which the ST will traverse the charged particle dense South Atlantic Anomaly (SAA), and consequently, ST would be put temporarily on gyro-hold without FGS use. However, concern arose over the effect of the more energetic galactic cosmic ray nuclei that would be present in that part of the ST's orbit outside of the Earth's radiation belts.

Since an attitude control simulation for the ST was under development, a logical step was to construct a model which simulated the photon noise caused by charged particles. This model, when installed in the ST attitude control simulation, would generate the photon counts in a random manner, whereby the impact of the charged particles on the allocated pointing error budget could be assessed.

Based on previous work in the area of photon detection by Teich, et al. [15-18], the first approach was to investigate the applicability of the Neyman Type-A distribution and the Thomas distribution which belong to the category of cluster (self-exciting) point processes. Cluster processes are characterized by a primary (mother) process which generates at each point secondary (daughter) events. When only daughter events appear in the final process and when primary and secondary distributions are both Poisson, the resulting distribution is known as the Neyman Type-A counting distribution with probability density function

$$P(n;p,s) = \sum_{m=0}^{\infty} \frac{(s\,m)^n}{n!}\, e^{-sm}\, \frac{p^m\, e^{-p}}{m!} \tag{30}$$

The parameter p represents the rate at which primary events occur and s is the average number of secondary counts per primary.

The Thomas distribution is similar, except that primary events are counted in the final process. The probability density function is given by

$$P(n;p,s) = \sum_{m=0}^{n} \frac{(s\,m)^{n-m}}{(n-m)!}\, e^{-sm}\, \frac{p^m\, e^{-p}}{m!} \tag{31}$$

It was soon recognized that the particle's path length through the PMT window [equations (17) and (19)] would be an important variable in any model attempting to estimate the photon counts caused by charged particles. As the setting became more complex, it was realized that a simulation would be required to unite all the relevant factors that would contribute to the photon noise. Secondly, the model could act as a forum from which the sensitivity of the parameters could be studied.

A computer program was written (Appendix F) to simulate charged particles striking the PMT window and the resultant Cerenkov radiation and fluorescence. Stereo visual computer graphics were particularly helpful in checking both the mathematics and programming during the modeling process

(Appendix D). The stereo pair in Figure 8 depicts the PMT window as struck by a charged particle (proton in this case) with entry point A and exit point B. Conically directed lines in Figure 9 show the cone of luminescence comprising the Cerenkov radiation. Figure 10 shows the paths of the fluorescence photons which follow after the Cerenkov radiation with a time constant of about .1 ms. Note the internal reflection. The computer graphics also pointed out the case in which the photocathode was struck by the fluorescence photons but not the Cerenkov radiation, demonstrating that the pulse amplitude of the Cerenkov photon noise is not a reliable warning of the subsequent fluorescence noise. Furthermore, the converse situation was also observed. This points out one of the difficulties in applying the Neyman or Thomas distribution, since sometimes the primary event (Cerenkov noise) is present in the final count, and sometimes not. However, in most applications, this would not pose a serious problem, since these two density functions have very similar properties.

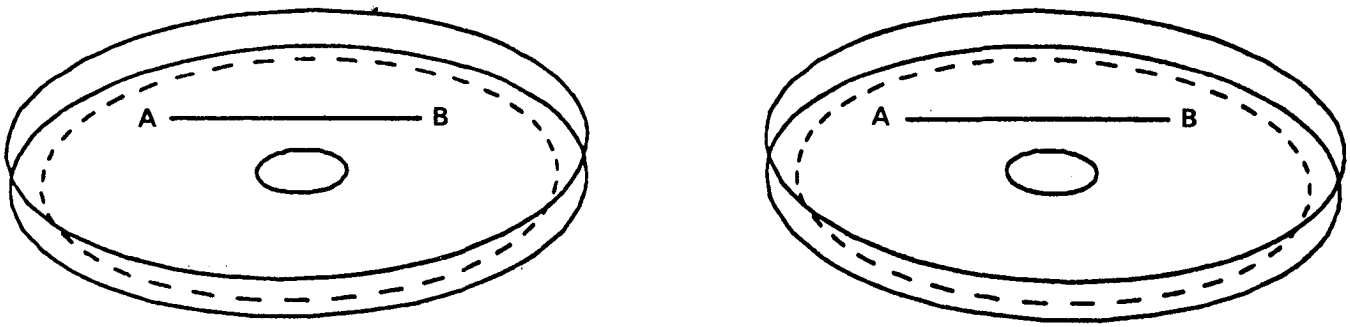

Figure 8. Proton striking the PMT window.

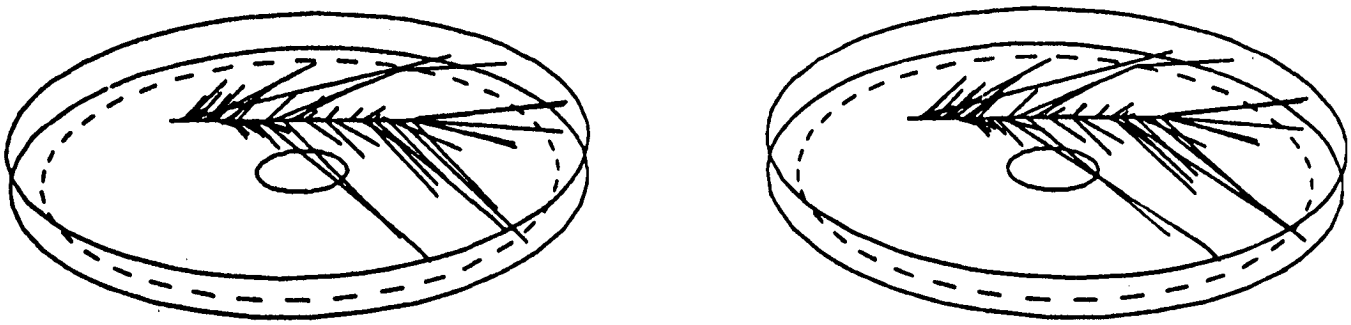

Figure 9. Cerenkov radiation caused by proton strike.

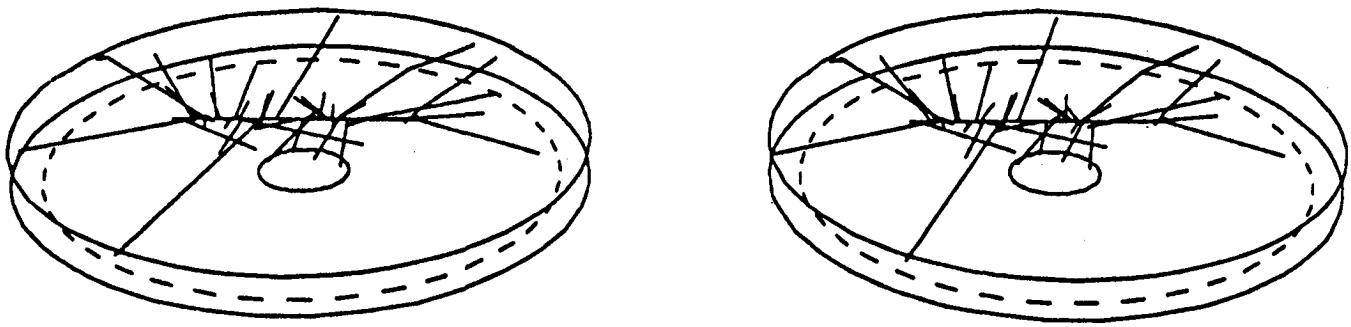

Figure 10. Fluorescence caused by proton strike.

A. Photon Noise Caused by Cosmic Ray Protons and Alpha Particles

Frequency statistics were computed for cosmic ray protons and alpha particles. Figure 11 shows the bivariate frequency distribution for Cerenkov radiation and fluorescence emitted in the PMT window caused by proton strikes. Figure 12a depicts the bivariate distribution for photon noise, i.e., those photons in Figure 11 which actually struck the effective photocathode region (Table 2 gives the numerical results). Figure 11, 12a, and 12b indicate poor correlation between Cerenkov and fluorescent yield at the photocathode and indicate poor efficiency for rejecting fluorescent events by the upper level threshold of the PMT PAD. Figure 12b shows the same information with the height magnified and the peaks at the origin clipped. These figures illustrate that very little of the radiation emitted along the charged particle's path actually strike the effective photocathode. This can be attributed to the following:

1) Small effective photocathode, i.e., it represents only one percent of the total area.

2) Photon loss because of transmission, absorption, and photon sink.

3) Photon loss because of the photocathode region outside of the effective area which make no contribution to the photon noise.

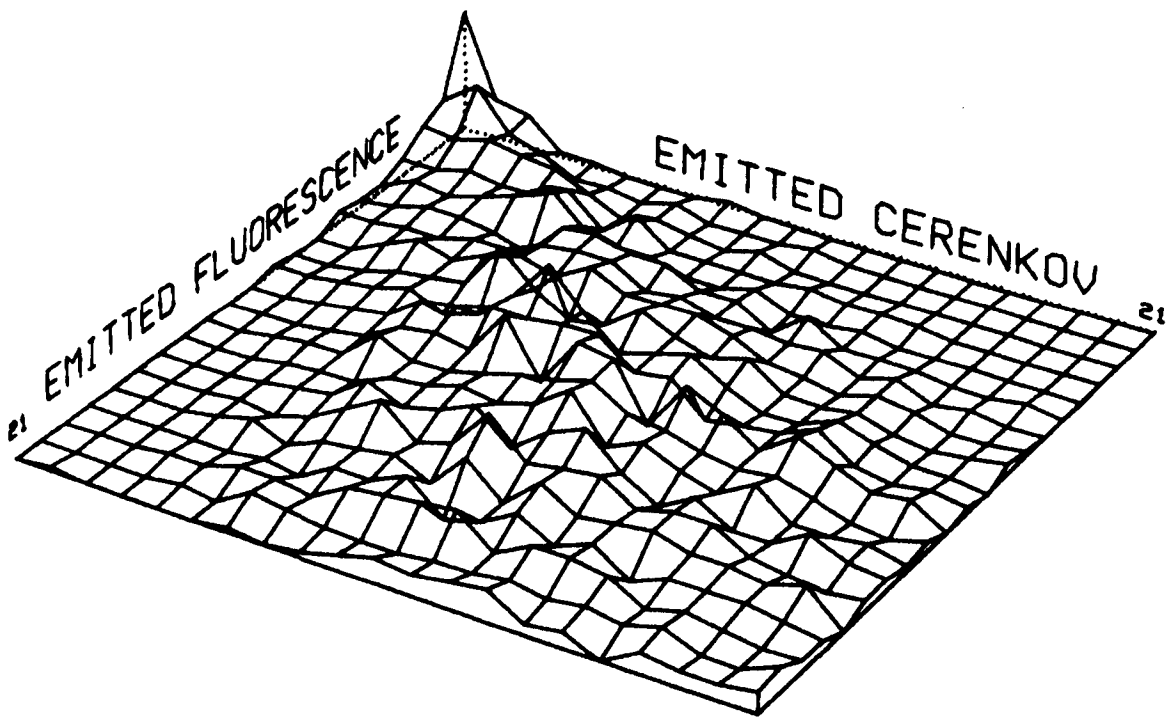

Figure 11. Bivariate frequency distribution of Cerenkov radiation and fluorescence emitted along the proton's path.

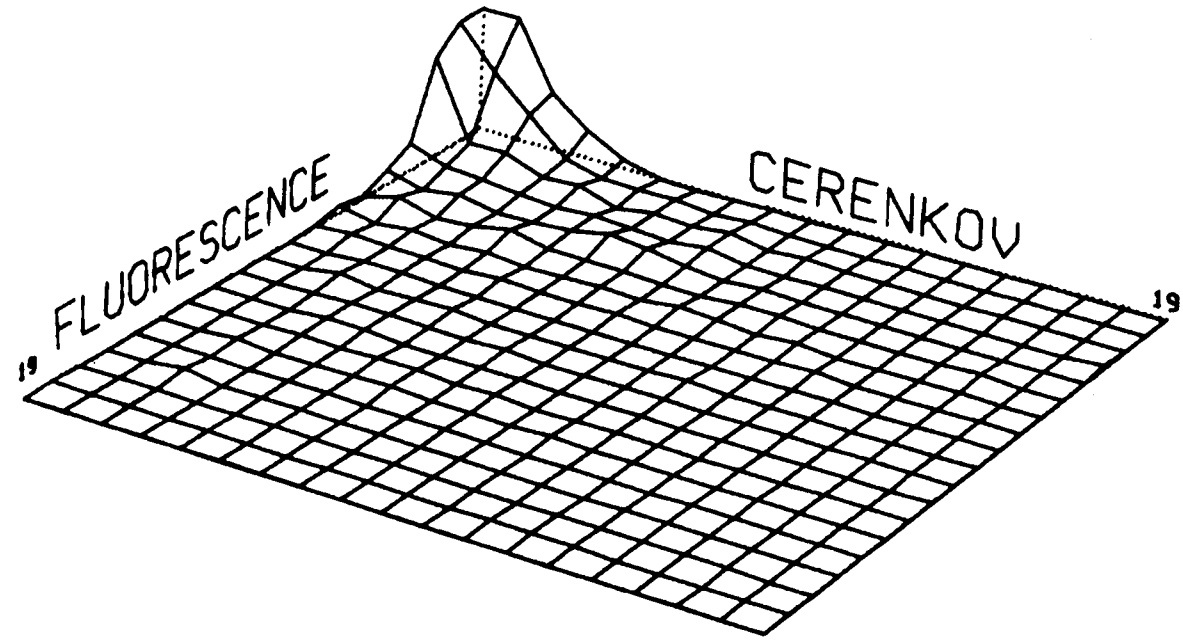

Figure 12a. Bivariate photon noise distribution.

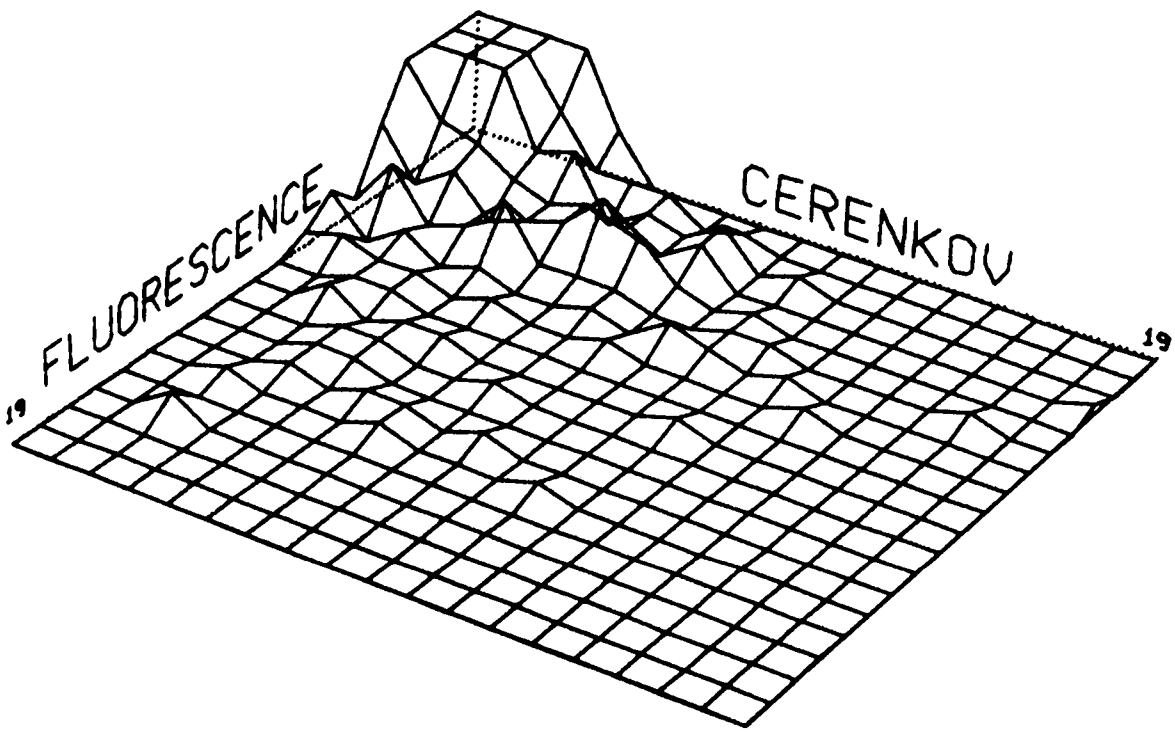

Figure 12b. Bivariate photon noise distribution magnified with peaks clipped.

TABLE 2. BIVARIATE FREQUENCY DISTRIBUTION OF PHOTON NOISE CAUSED BY 2507 SIMULATED PROTON STRIKES

Cerenkov Noise	Fluorescence Noise																			
	0	1	2	3	4	5	6	7	8	9	10	11	12	13	14	15	16	17	18	
0	1894	213	40	11	6	1	3	1	0	0	0	0	0	0	0	0	0	0	0	2169
1	92	33	10	6	2	5	0	2	0	0	0	0	0	0	0	0	0	0	0	150
2	23	20	10	5	4	1	2	1	1	2	0	0	0	1	0	2	0	0	0	72
3	12	6	4	3	1	2	0	1	1	0	1	1	1	0	0	0	0	0	0	33
4	4	2	5	2	2	5	1	0	0	1	1	1	0	0	0	0	0	0	0	24
5	0	2	0	3	3	1	0	1	0	1	0	0	1	0	0	0	0	0	0	12
6	0	2	2	2	6	1	0	0	0	0	0	0	1	1	0	0	0	0	0	15
7	0	0	1	1	4	1	1	0	0	0	1	0	0	0	0	0	0	0	0	9
8	0	1	3	3	1	0	0	1	0	0	0	0	1	0	0	0	0	0	0	10
9	0	0	0	0	0	0	2	0	0	0	0	0	0	0	0	0	0	0	0	2
10	0	0	1	0	1	1	1	0	0	0	0	0	0	1	0	0	0	0	0	5
11	0	0	0	0	0	1	0	0	0	1	0	0	0	0	0	0	0	0	0	2
12	0	0	0	0	0	0	1	0	0	0	0	0	0	0	0	0	0	0	0	1
13	0	0	0	0	0	0	0	1	0	0	0	0	0	0	0	0	0	0	0	1
14	0	0	0	0	0	0	0	0	0	0	0	0	0	0	0	0	0	0	0	0
15	0	0	0	0	0	0	0	0	0	0	0	0	0	0	0	0	0	0	0	0
16	0	0	0	0	0	1	0	0	0	0	0	0	0	0	0	0	0	0	0	1
17	0	0	0	0	0	0	0	0	0	0	0	0	0	0	0	0	0	0	0	0
18	0	0	0	1	0	0	0	0	0	0	0	0	0	0	0	0	0	0	0	1
	2025	279	76	37	30	20	11	8	2	5	3	2	4	3	0	2	0	0	0	2507

Figures 13a and 13b represent the probability density functions for Cerenkov noise and fluorescence noise obtained for cosmic-ray proton strikes. The mean number of simulated Cerenkov counts caused by proton strikes is 0.37. For comparison with experimental results, the inset figure is included where those strikes which yielded zero counts were ignored (since the multiplier photo tube recognizes only those photons which strike the photocathode). Thus, the mean obtained when zeros are omitted is 2.75. The mean of the fluorescence density function is 0.423 (zeros included) and 2.21 when zeros are omitted. The numerical values of the PDF and CDF (probability and cumulative density function, respectively) are given in Table 3.

Figures 14a and 14b are the simulated probability density functions for alpha particle photon noise, with means 1.47 and 6.34 (zeros omitted) for Cerenkov noise and 1.16 and 3.10 for fluorescence noise. Table 4 provides the numerical values of the noise PDF and CDF for alpha particle fluorescence. Figure 15 depicts the simulated probability density function for the length of the charged particle's path through the PMT window. Figure 16 is the distribution of emitted Cerenkov photons caused by proton strikes and Fig. 17 is the distribution of emitted fluorescence.

One proposed method for eliminating the effect of fluorescence is to recognize the Cerenkov pulse amplitude height (proportional to the number of Cerenkov photons which strike the photocathode) and then blank the PMT counter for the next millisecond, thereby eliminating the majority of the unwanted fluorescence noise.

However, the simulation points out that it often is the case that fluorescence noise is produced without Cerenkov photons having struck the photocathode. This may be largely attributed to the directed nature of the Cerenkov radiation in which photons exit the window with little or no internal reflection but the fluorescence photons, in their more random flights, eventually strike the photocathode either directly or after reflection.

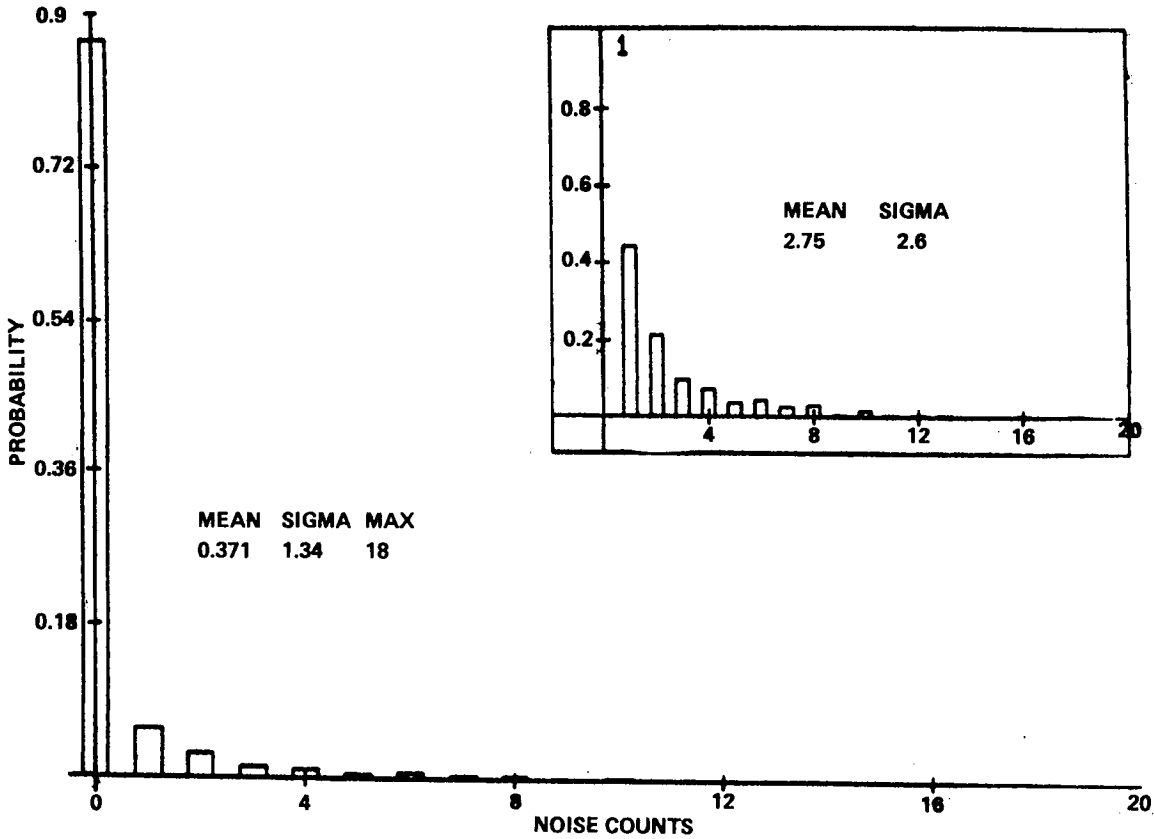

Figure 13a. Probability density function of Cerenkov noise caused by protons.

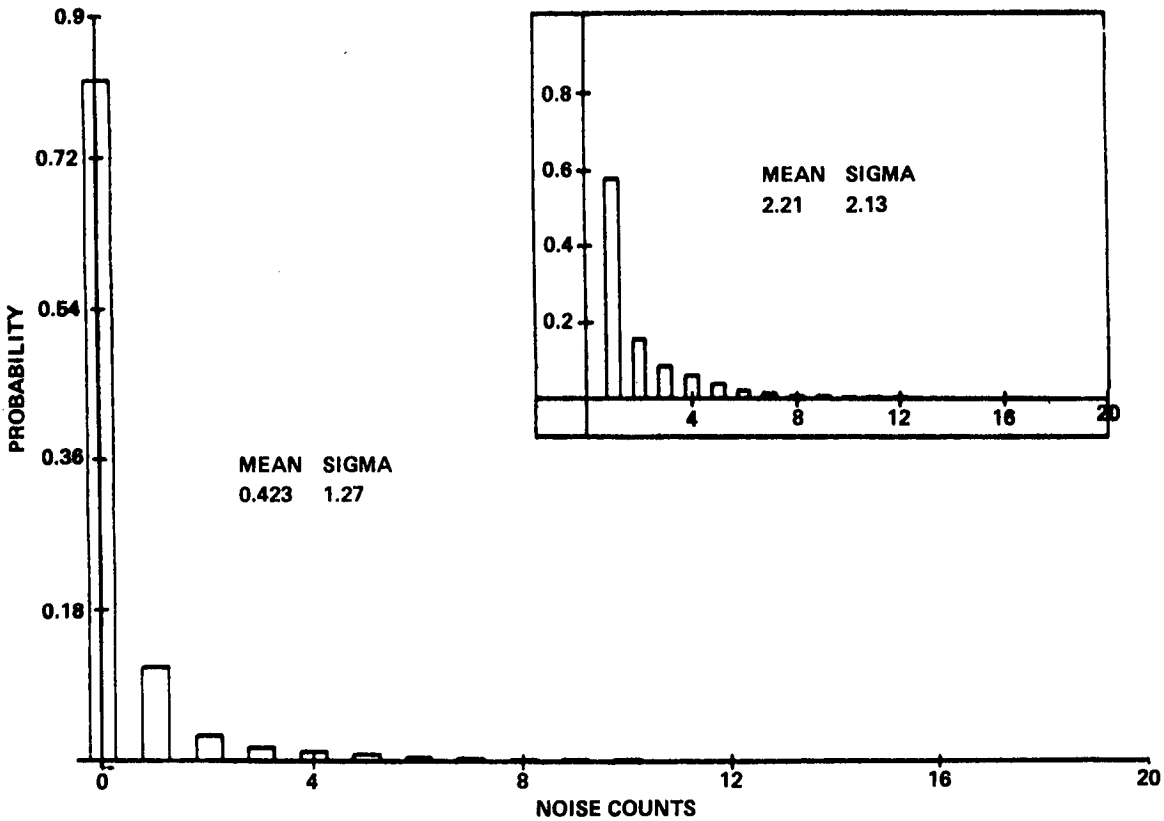

Figure 13b. Probability density function of fluorescence noise caused by protons.

TABLE 3. FLUORESCENCE NOISE DISTRIBUTION CAUSED BY PROTONS

PHOTON NOISE	PDF	CDF
0	0.808167	0.808167
1	0.111347	0.919515
2	0.030331	0.949846
3	0.016726	0.966572
4	0.011449	0.978021
5	0.007982	0.986003
6	0.004390	0.990393
7	0.002796	0.993189
8	0.001755	0.994944
9	0.001386	0.996330
10	0.001100	0.997430
11	0.000752	0.998182
12	0.000662	0.998844
13	0.000525	0.999368
14	0.000370	0.999739
15	0.000261	1.000000

TABLE 4. FLUORESCENCE NOISE DISTRIBUTION CAUSED BY ALPHA PARTICLES

PHOTON NOISE	PDF	CDF
0	0.626020	0.626020
1	0.187483	0.813502
2	0.075424	0.888926
3	0.033957	0.922883
4	0.016864	0.939747
5	0.011549	0.951296
6	0.009497	0.960793
7	0.007069	0.967862
8	0.005428	0.973290
9	0.003788	0.977079
10	0.002900	0.979979
11	0.002415	0.982394
12	0.002054	0.984448
13	0.001709	0.986157
14	0.001449	0.987606
15	0.001173	0.988780
16	0.001007	0.989787
17	0.000860	0.990647
18	0.000802	0.991449
19	0.000747	0.992196
20	0.000677	0.992873
21	0.000628	0.993501
22	0.000596	0.994098
23	0.000596	0.994694
24	0.000551	0.995245
25	0.000522	0.995767
26	0.000507	0.996275
27	0.000480	0.996754
28	0.000466	0.997220
29	0.000426	0.997646
30	0.000388	0.998035
31	0.000340	0.998375
32	0.000306	0.998681
33	0.000284	0.998966
34	0.000252	0.999218
35	0.000222	0.999440
36	0.000212	0.999652
37	0.000183	0.999835
38	0.000165	1.000000

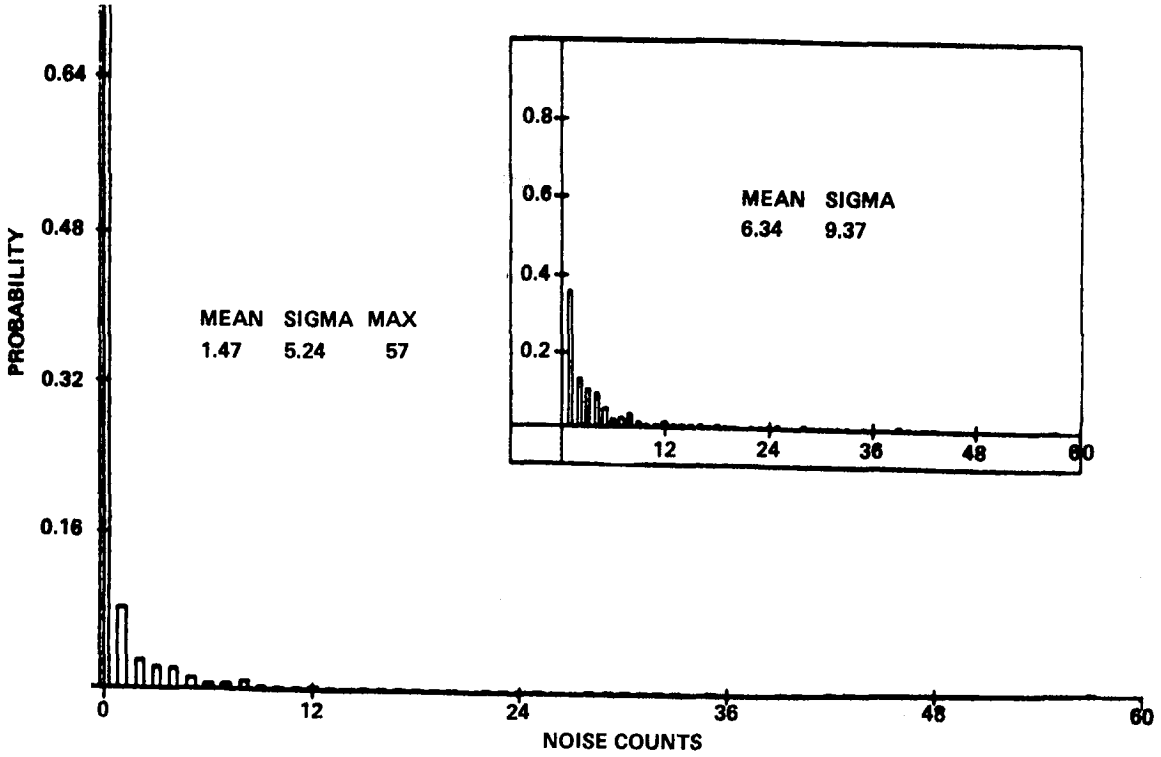

Figure 14a. Probability density function of Cerenkov noise caused by alpha particles.

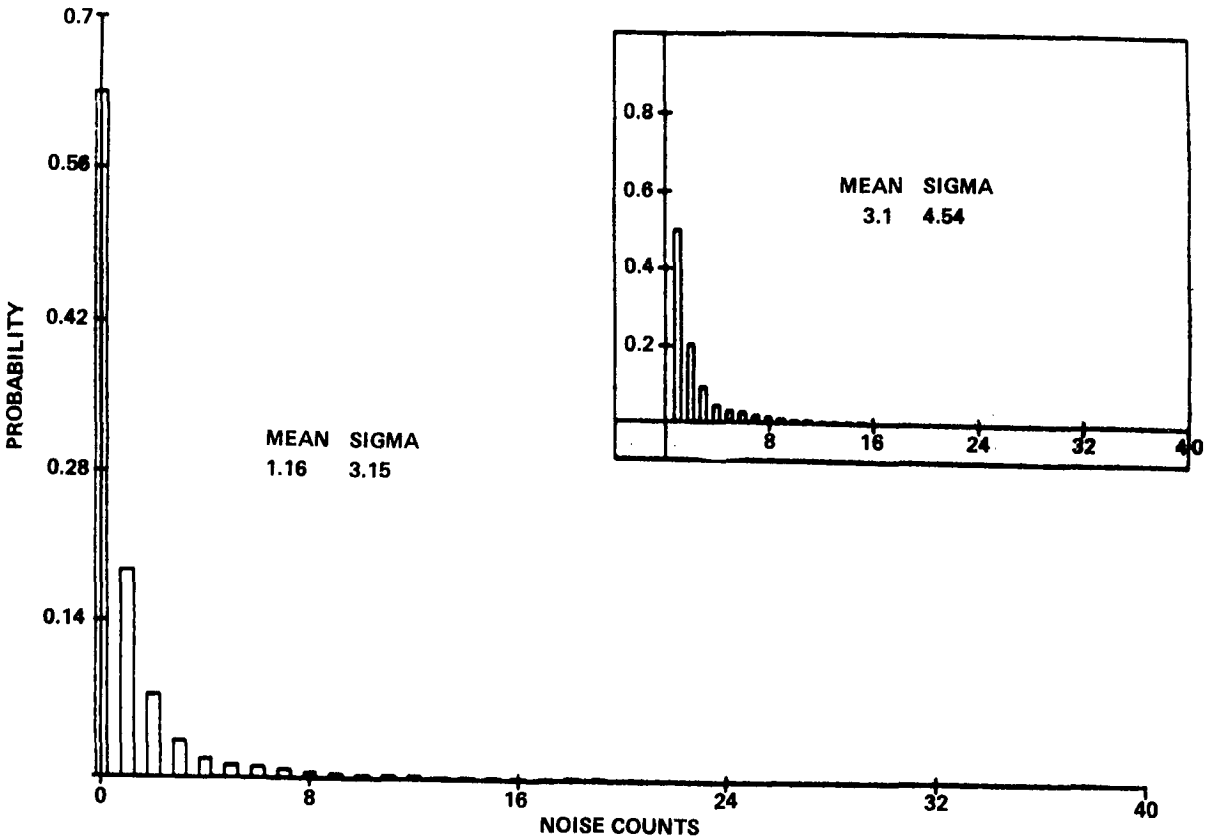

Figure 14b. Probability density function of fluorescence noise caused by alpha particles.

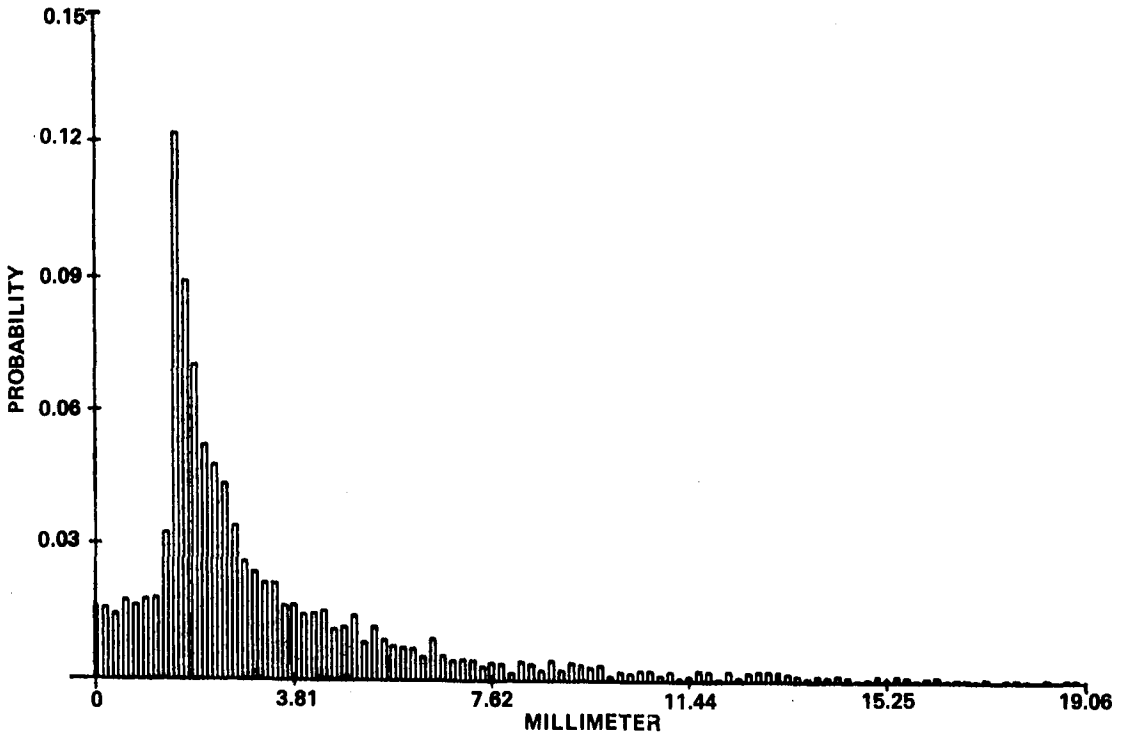

Figure 15. Distribution of the charged particle's pathlength through the PMT window.

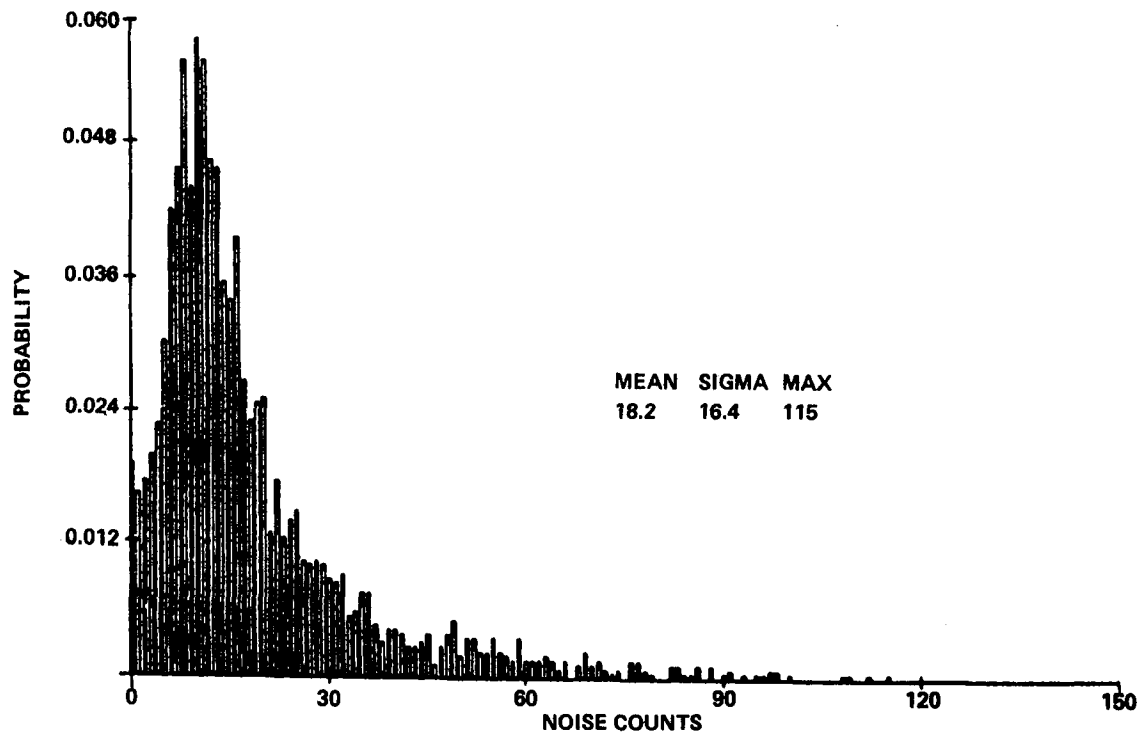

Figure 16. Distribution of the emitted Cerenkov photons caused by proton strikes.

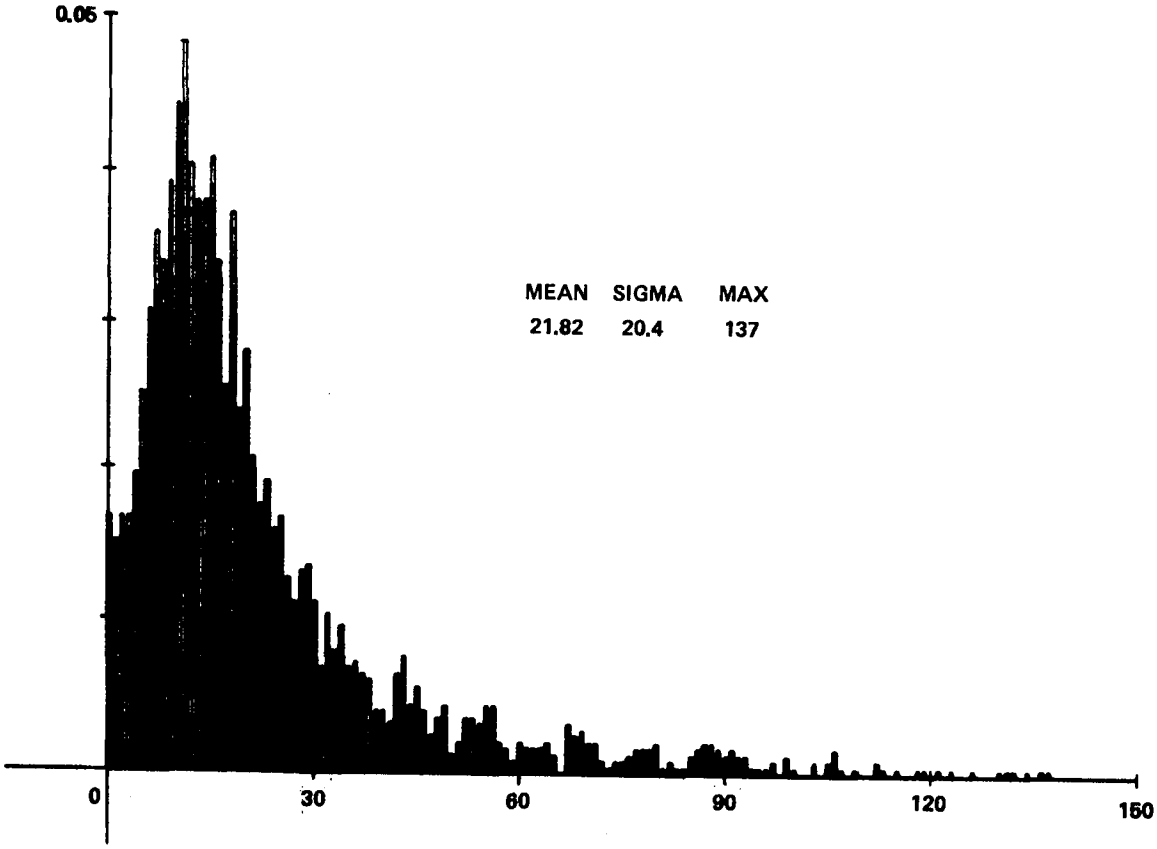

Figure 17. Distribution of emitted fluorescence photons caused by proton strikes.

B. SAA Protons and Alpha Particles

The difference between protons and alpha particles trapped in the SAA and the cosmic ray nuclei is their energies. The cosmic ray nuclei's energy is on the order of magnitude of a BeV whereas SAA particle energies are on the order of magnitude of a MeV. Particles with energy less than 300 MeV contribute no Cerenkov radiation [$\theta = 0$ in equation (20)] while the stopping power term dE/dX appearing in equation (19) has its minimum mean value at around 1 BeV, increasing sharply for less energetic particles.

Consequently, the amount of Cerenkov radiation will be quite small and fluorescence abundant during the time in which ST will traverse the SAA.

As expected, simulation studies for both SAA protons and alpha particles resulted in negligible amounts of Cerenkov radiation and large amounts of fluorescence.

C. Parameter Study of PMT Window Height

Also of interest were the effects of changing the PMT window dimensions. Comparisons were made for cosmic ray protons with the PMT window radius remaining fixed and the height (thickness) varied.

Since the number of Cerenkov photons and fluorescence photons is proportional to the charged particle's path length through the window, it seemed intuitive that the number of photon noise counts

would increase with the increased window size. However, simulated means of Cerenkov and fluorescence monotonically decreased as the height increased. The apparent anomaly can be attributed to the fact that the window's surface area increases more rapidly than the window's linear dimensions, meaning that although more photons are produced by the charged particle, there is even less likelihood that they will strike the photocathode since the ratio of the area of the photocathode to the window surface area is decreasing at a rate faster than the mean charged particle path length is increasing.

Since we are working only with the distribution of induced counts, conditional on having a charged particle strike, it is difficult to assess the value of this result since clearly the rate of charged particle strikes increases as the size of the PMT window increases. Thus, one would need to work out the multivariate problem when searching for an optimal PMT window size.

D. Comparison with Experimental Results

An experiment was conducted by the Space Science Laboratory at Marshall Space Flight Center to measure the photon noise with the use of a multiplier photo tube identical to the one we modeled. A beam of muons was selected by a separate detector in coincidence with the top of the PMT window and a mean of three counts was recorded for Cerenkov radiation and two for fluorescence.

The appropriate parameters were adjusted in the model to simulate charged particles striking the top of the PMT window. Directions cosines of the particle's path were modeled as follows:

1) The angle θ of incidence (angle measured from the window top normal) was assumed to follow a distribution

$$f(\theta) = \frac{24}{\pi} \cos^2 6\theta \qquad , \qquad 0 \leqslant \theta \leqslant \pi/12$$

where experimental evidence suggested that $f \propto \cos^{1.6}$ [5]. For mathematical convenience, we used the $\cos^2$ function.

2) The azimuth angle was assumed to be uniform $(0,2\pi)$.

The simulated means were 4.5 and 1.7 for Cerenkov and fluorescence counts, respectively, zeros having been suppressed. The ratios of the simulated means for the space environment to the simulated means of the experimental set-up are 0.53 for Cerenkov counts and 1.33 for fluorescence. The experiments performed with muons in the laboratory have large estimated errors (± 50 percent) in Cerenkov and fluorescence yields. Therefore, the means obtained from the simulation are compatible with the experimental values. An accelerator experiment using particles with a high charge number would be required to perform a definitive comparison. Such an experiment would yield an accurate value for the fluorescent efficiency.

Simulated means for Cerenkov noise (C) and fluorescence noise (F) of the lab experiment and the space environment for cosmic-ray protons is given below:

	Simulation of Lab Experiment		Simulation of Space Environment	
	C	F	C	F
Zero counts included	0.27	0.23	0.22	0.43
Zeros deleted	4.5	1.7	2.4	2.2

The higher rate of Cerenkov radiation in the simulation of the lab experiment may be explained in that the charged particles are directed at the PMT window from above. Thus the Cerenkov radiation is directed conically towards the effective photocathode region. In the space environment, equal numbers of particles would be expected to enter the window through the bottom as well as the top. Cerenkov radiation emitted by charged particles entering from the bottom would be directed out of the top, with very little being reflected and then striking the photocathode.

IV. CONCLUSIONS

A stochastic model for Cerenkov radiation and fluorescence resulting from the direct interaction of a charged particle with the multiplier phototube window has been developed. This model simulates the bivariate probability density function for the number of Cerenkov photons and fluorescence photons which strike the effective photocathode region which contribute to photon noise. It is applicable to charged particles trapped in the Earth's radiation belts and to the more energetic cosmic ray nuclei. The model's parameters were adjusted to correspond with the physical environment of an experiment designed to estimate photon noise caused by cosmic ray protons. Experimental mean counts corresponded very well with the model's prediction, thereby justifying a certain degree of confidence in the model's ability to predict.

The density functions for fluorescence noise obtained from the simulation of cosmic ray nuclei and alpha particles (Tables 1 and 2) have been inserted into the ST Fine Guidance Sensor model to provide randomly generated photon noise in the FGS simulation. This allows for the evaluation of their effect on the overall ST pointing error budget.

A simulation of carbon nuclei strikes was also conducted and the resultant bivariate histogram of Cerenkov noise and fluorescence noise clearly pointed out that the Cerenkov pulse amplitude height could not reliably be used to signal the associated fluorescence noise. A limit was therefore placed on the error of the Fine Guidance Sensor interferometer signal. This limit minimizes the effect of the strikes.

Variation of the PMT geometry showed that the average fraction of the total number of photons which intercepted the photocathode decreased as the thickness of the PMT window was increased. This, together with an accurate model for the rate at which charged particles strike a PMT window as a function of window dimensions could be applied in the design of multiplier phototubes. The model will also be used to simulate various charged particle/glass interaction experiments in astrophysics.

APPENDIX A

UNIFORM RANDOM NUMBER GENERATOR

The advent of high-speed digital computers has made it possible to use simulation techniques incorporating probabilistic features. These simulations are generally called Monte Carlo simulations and are resorted to whenever the system being studied is not amenable to analytical methods. An integral part of these simulations is the use of random numbers having a certain specified distribution characteristic of the process being studied.

The basic element of all Monte Carlo simulations is the uniform random-number generator. Once uniform random numbers are available, all other desired distributions can be obtained either by use of the probability integral transformation or by applying some known relationship between the desired distribution to be generated and the uniform distribution.

One of the most widely used uniform random number generators today is the congruential type first proposed by D. H. Lehmer in 1949 [19]. Accordingly, the random number generator takes the form

$$X_{i+1} = (A\ X_i + B)\ \text{Mod}\ M \quad , \quad i = 0,1,2, \ldots \tag{A-1}$$

where A, B, and M are integers and X_0 is a "seed" number. Since the congruential relationship is cyclical, the sequence of random numbers will repeat after a certain period. The statistical behavior of the generated random numbers is predominantly governed by the choice of the multiplier A and the modulus M. Therefore, the most widely used generators are of the type B = 0. Many empirical and theoretical tests have been developed to assess the "goodness" of random number generators. Based on a test called the lattice test [20], Carroll [21] found the congruential generator with A = 29,903,947 and $M = 2^{31} - 1$ to be a satisfactory generator for the computer on which we would run the simulation.

APPENDIX B

GENERATION OF RANDOM NUMBERS FROM NON-UNIFORM DISTRIBUTIONS

Many of the generators for continuous distributions are a direct application of the probability integral transformation [22]. For a given uniform random number U between zero and one, a random number X having a desired distribution F(X) can be obtained by solving the equation U = F(X) for X. Since this process requires the determination of the inverse of the cumulative distribution function, its practicality depends upon the availability of explicit expressions or convenient approximations for this inverse cumulative distribution function. Generation of random numbers from discrete distributions is handled in a manner analogous to that of continuous distributions. Given a uniform random number U and cumulative discrete distribution F(X), we seek the least value of X for which $F(X) \geqslant U$. This X is the desired random number having discrete probability density function f(x).

APPENDIX C

UNIFORM DISTRIBUTION OVER THE SURFACE OF A SPHERE

Lacking any information to the contrary, we have assumed that the direction of a charged particle's path is uniformly distributed. This is sometimes called the postulate of equal apriori probabilities. The direction can be expressed by direction cosines and our goal was to select these in such a way that each surface element of a unit sphere has equal probability of containing the unit vector tip obtained from the direction cosines of the particle's path. The azimuth angle ϕ is taken to be uniformly distributed from 0 to 2π. The elevation angle is determined by observing that the area of a band (width determined by an angle θ) around the surface of a unit hemisphere is given by $2\pi \sin \theta$ (Fig. C-1). The requirement that the surface elements be equi-probable gives

$$\Pr(\Theta \leqslant \theta) = (2 \pi \sin \theta)/2 \pi = \sin \theta \tag{C-1}$$

which is the cumulative distribution function for the elevation angle. From equation (C-1) we get

$$\theta = \sin^{-1} U \tag{C-2}$$

as the desired random elevation. To generate points on the surface of a sphere, we let U range from -1 to +1. Thus, the direction cosines are given by

$$\begin{bmatrix} d_1 \\ d_2 \\ d_3 \end{bmatrix} = \begin{bmatrix} \sqrt{1 - \sin^2 \theta} \cos \phi \\ \sqrt{1 - \sin^2 \theta} \sin \phi \\ \sin \theta \end{bmatrix}$$

where $\phi = 2\pi U_1$ and $\sin \theta = 2(U_2 - 0.5)$, where U_1 and U_2 are independent random numbers uniformly distributed between -1 and 1.

Figure C-2 demonstrates points uniformly distributed on the surface of a hemisphere.

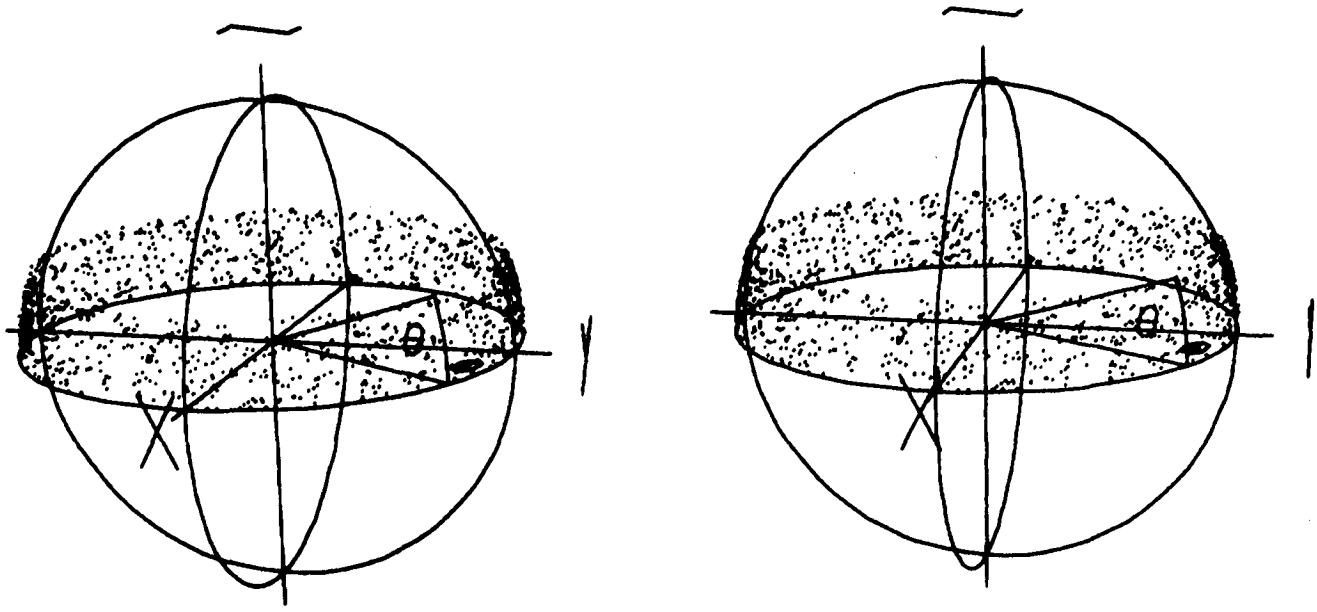

Figure C-1. Unit hemisphere.

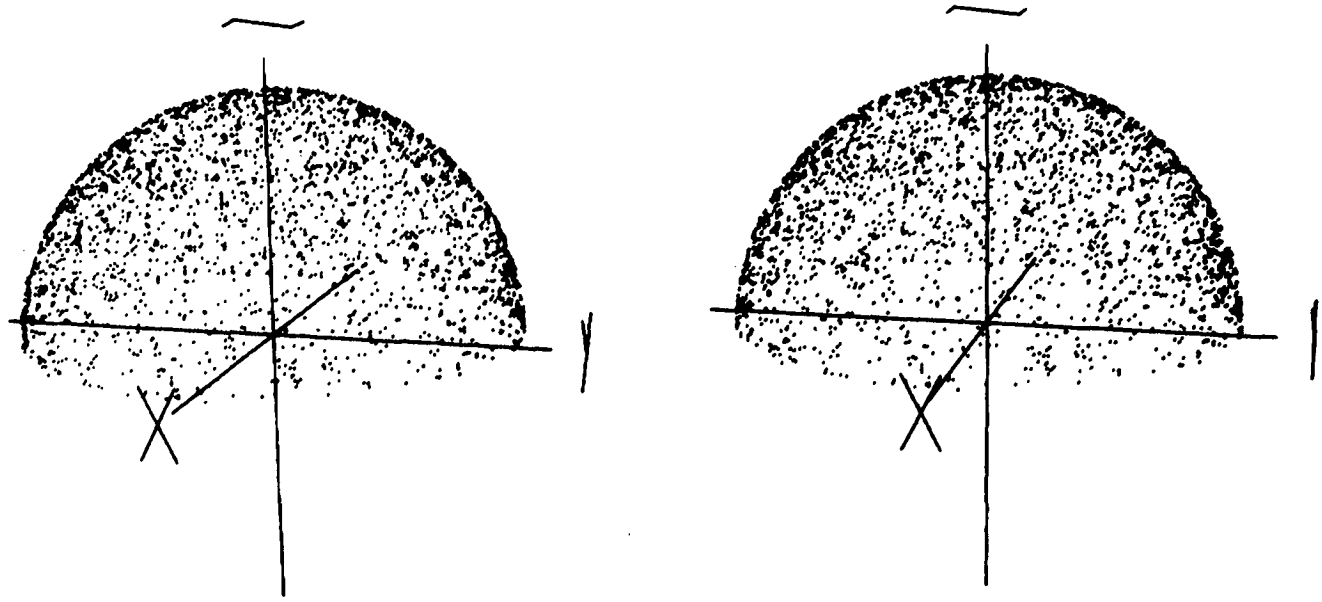

Figure C-2. Uniform distribution over a hemisphere.

APPENDIX D

STEREO VISUALIZATION WITHOUT OPTICAL AIDS

(Cross-eyed Stereo)

On many occasions in engineering and physical analysis it is useful to be able to sketch in three dimensions. To fulfill this wish in many cases, we have used a convenient technique which requires no optical devices other than one's eyes. All that is required is a stereoscopic pair of images. One additional capability is necessary. The observer must be able to cause the lines of sight of his eyes to converge; i.e., one must cross one's eyes. The stereo projections are formed as shown in Figure D-1. The images are reversed and viewed as in Figure D-2. With a little practice, one can easily learn to reconstruct mentally, the 3-dimensional scene from the reversed stereo pairs. The interested reader should try several viewing distances (the farther away the page the less crossing of the eyes is required and the easier it becomes to focus the images). Squinting may also help as it increases one's depth of focus. When one first looks at a stereo pair, one focuses on the page and sees two similar but separate images. As one begins to cross his eyes, the two images become four. Continue crossing the eyes until the interior pair of images come together. Since the line connecting corresponding points on the images must be at the same angle about the line of sight as the line connecting the eyes, it may be necessary to rotate the page or rock the head until these two images become superimposed and seem to merge into a stereo image. This technique does require some practice but once mastered it can be very useful for easy visualization in 3 dimensions.

If a computer with plot capability is available, we can construct the necessary stereo projections from a set of points and lines that represent the object of interest. We have referred to such a representation as a wire frame model because of the appearance of the image. Let P be a representative point of the model. Each point P is projected into the picture plane S as shown in Figure D-3. The point P is projected to the eyepoint E and the line PE intersects the picture plane S at P′. P′ is the projection of P onto S. The set of all points P′ projected from object points P together with the connecting lines form the desired projection. We set up a reference frame in the plane S. To do this, we must specify which way is up (so to speak). Let $\underline{u}_u$ be a unit vector in this direction and $\underline{u}_r = \underline{u}_u \times \underline{\ell}$ is a unit vector in S pointing to the right. We place the origin of the S coordinate reference at O. Observe that $\underline{r}_O = \underline{r}_E + d\,\underline{\ell}$; where $\underline{r}_O$ and $\underline{r}_E$ are position vectors of O and E respectively. From the geometry shown in Figure D-3, we can see that

$$\underline{r}_{P'} = \underline{r}_E + (\underline{r}_P - \underline{r}_E)\, d/\underline{\ell} \cdot (\underline{r}_P - \underline{r}_E) \quad .$$

From this we can compute

$$x_{P'} = (\underline{r}_{P'} - \underline{r}_O) \cdot \underline{u}_r$$

$$y_{P'} = (\underline{r}_{P'} - \underline{r}_O) \cdot \underline{u}_u$$

Since

$$\underline{\ell} \cdot \underline{u}_u = \underline{\ell} \cdot \underline{u}_r = 0 \quad ,$$

$$x_{P'} = (\underline{r}_{P'} - \underline{r}_E) \cdot \underline{u}_r$$

$$y_{P'} = (\underline{r}_{P'} - \underline{r}_E) \cdot \underline{u}_u \quad .$$

The set of points $(x_{P'}, y_{P'})$ plotted conventionally forms the desired projection. Size can be altered by scale adjustments. These projections are then placed as desired. Also, the values used for d and eye separation s are arbitrary and can be adjusted for convenience or eye comfort. In real life s $\cong$ 65 mm and d $\cong$ 250 mm for comfortable reading; however, it may be more comfortable for d to be larger. Some initial experimentation with this technique should establish desireable settings.

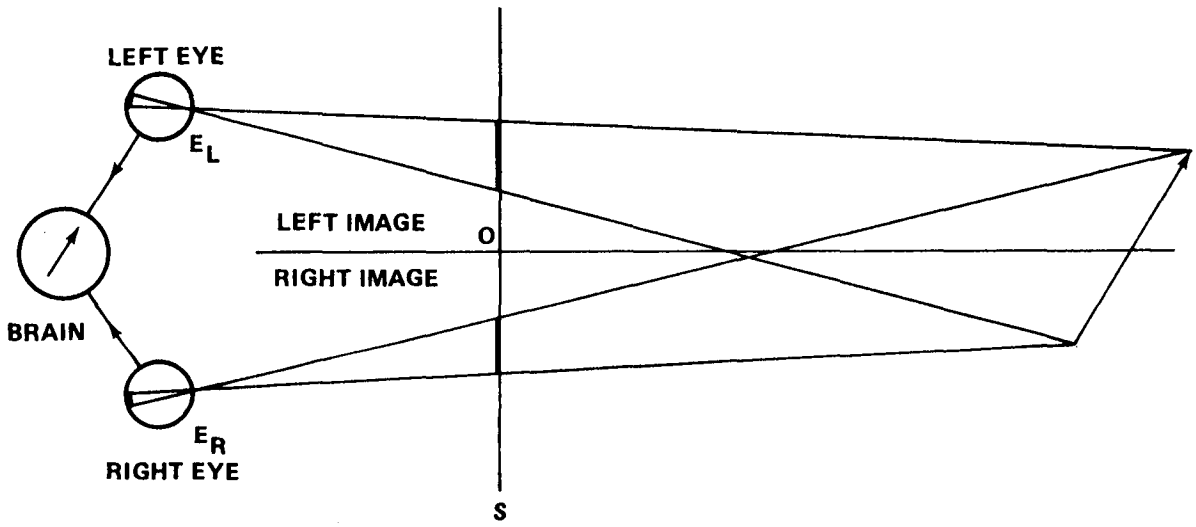

Figure D-1. Stereo projection.

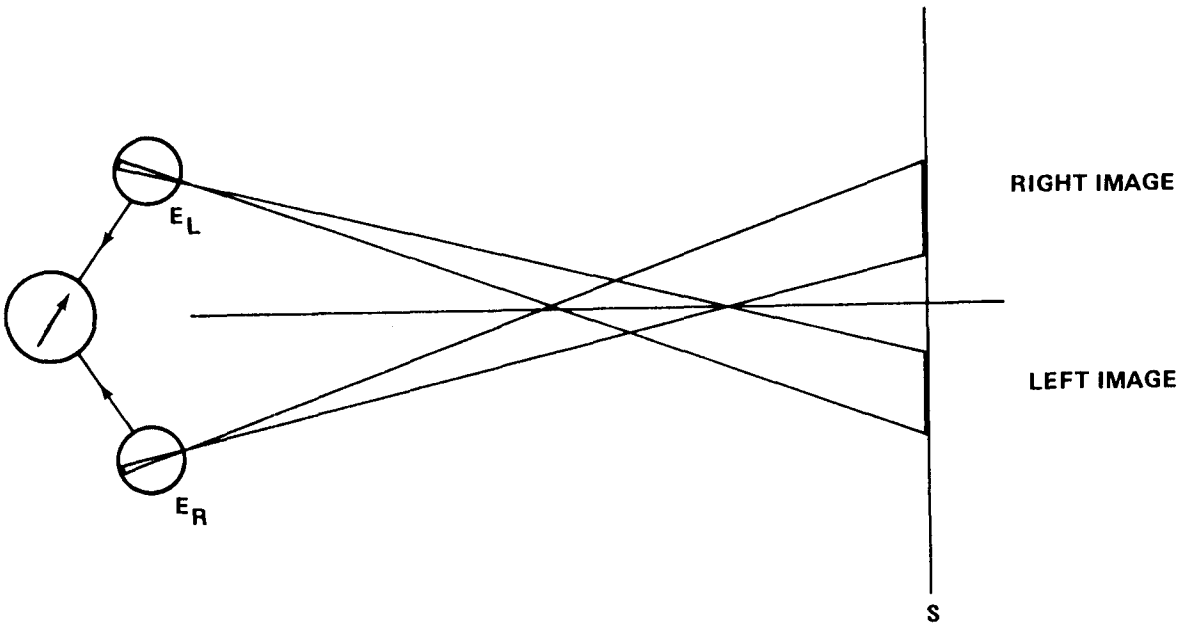

Figure D-2. Stereo reconstruction.

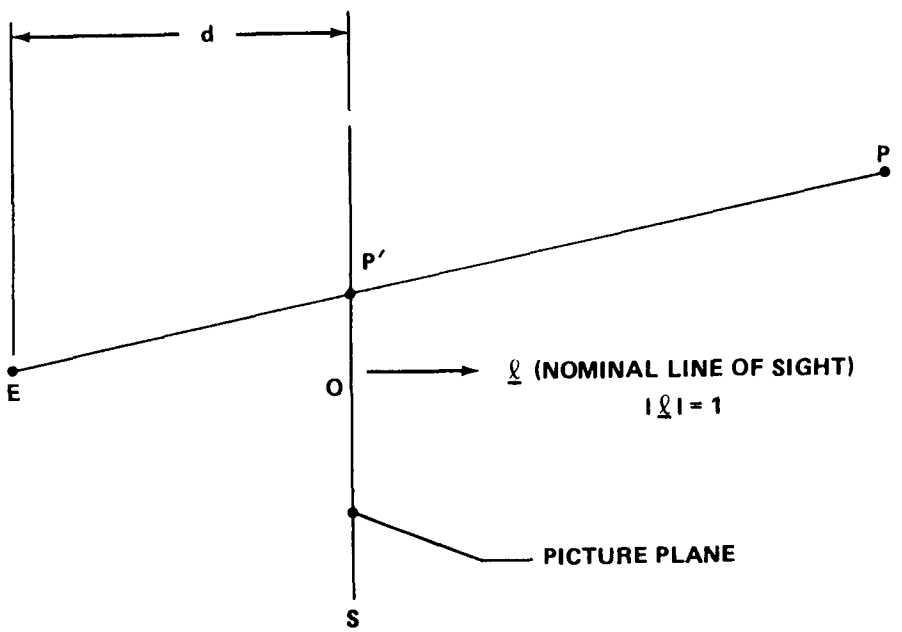

Figure D-3. Projection geometry.

APPENDIX E

RESTRICTED ENERGY LOSS DISTRIBUTION

The stopping power or mean energy lost per unit pathlength in a medium by a charged particle is proportional to the particle's nuclear charge squared. However, the stopping power is only the average energy lost to the absorber. Identical particles with the same trajectory will produce a distribution of energy losses often referred to as "straggling." This variation in energy loss is the result of the finite number of events that occur in the ionization energy loss process.

The stochastic variation of the energy lost to a thin absorber by a charged particle was first attacked by Landau [23]. His derivation assumes that only a small fraction of the particle's initial energy is lost and no upper limit is placed on the amount of energy which may be transferred to a single electron.

Vavilov [24] obtained a more rigorous solution without the approximation of unbounded single energy transfers.

Watts [25] makes the distinction that energy loss depends on the type of material and energy deposited depends on the surrounding geometry as well.

Under the assumption that all electrons with energy below ϵ_1 deposit their energy in the volume element where they are produced, energy loss becomes equivalent to energy deposition. Energies above ϵ_1 are transported out of the region by scattering of electrons and are referred to as delta rays.

The probability density function for energy loss Δ over a pathlength of x cm is given by [25]

$$f(\Delta;x) = \frac{1}{\pi\epsilon_1} e^{\frac{\kappa(1 + \epsilon_1 \beta^2 \gamma)}{\epsilon_{max}}} \int_0^\infty e^{\kappa g_1(u)} \cos [\lambda u + \kappa g_2(u)] \, du \qquad \text{(E-1)}$$

where $\kappa = x\xi/\epsilon_1$, ϵ_1 is the cutoff energy, and ϵ_{max} is the maximum possible energy transferred to an electron given by

$$\epsilon_{max} = \frac{2 M_e c^2 \beta^2}{1 - \beta^2} \left[1 + \frac{2 M_e}{M_P \sqrt{1 - \beta^2}} + \left(\frac{M_e}{M_P} \right)^2 \right]^{-1} ,$$

$$\xi = \frac{2\pi N_o Z^2 e^4}{M_e c^2 \beta^2} ,$$

$$\lambda = \frac{\Delta - \overline{\Delta}}{\epsilon_1} - \kappa \left(\ln \frac{\epsilon_1}{\epsilon_{max}} + \beta^2 + 1 - \gamma \right) ,$$

where γ is Euler's constant 0.577215665;

$$g_1(u) = \frac{\epsilon_1 \beta^2}{\epsilon_{max}} [\ln u - Ci(u)] - u\, Si(u) - \cos(u) \quad , \tag{E-2}$$

$$g_2(u) = u\, [\ln u - Ci(u)] + \frac{\epsilon_1 \beta^2}{\epsilon_{max}} Si(u) + \sin u \quad . \tag{E-3}$$

Other terms are as follows:

Ci is the cosine integral approximated by:

$$Ci(u) = \begin{cases} \gamma + \ln u & u \leqslant 0.01 \\ \gamma + \ln u + \sum_{j=1}^{\infty} \frac{(-1)^j u^{2j}}{(2j)!2j} & 0.01 < u < 1.0 \\ G(u) \sin u - H(u) \cos u & 1.0 \leqslant u < 50.0 \\ \frac{\sin u}{u} & u \geqslant 50.0 \end{cases} \tag{E-4}$$

and the sine integral is approximated by

$$Si(u) = \begin{cases} u & u \leqslant 0.01 \\ \sum_{j=0}^{\infty} \frac{(-1)^j u^{2j+1}}{(2j+1)!(2j+1)} & 0.01 < u < 1.0 \\ \pi/2 - G(u) \cos u - H(u) \sin u & 1.0 \leqslant u < 50.0 \\ \pi/2 - \frac{\cos u}{u} & u \geqslant 50.0 \end{cases} \tag{E-5}$$

where

$$G(u) = \frac{1}{u} \left(\frac{u^8 + a_1 u^6 + a_2 u^4 + a_3 u^2 + a_4}{u^8 + a_5 u^6 + a_6 u^4 + a_7 u^2 + a_8} \right) \tag{E-6}$$

$$H(u) = \frac{1}{u^2}\left(\frac{u^8 + b_1u^6 + b_2u^4 + b_3u^2 + b_4}{u^8 + b_5u^6 + b_6u^4 + b_7u^2 + b_8}\right) \qquad \text{(E-7)}$$

and

$a_1 = 38.027264$

$a_2 = 265.187033$

$a_3 = 335.677320$

$a_4 = 38.102495$

$a_5 = 40.021433$

$a_6 = 322.624911$

$a_7 = 570.236280$

$a_8 = 157.105423$

$b_1 = 42.242855$

$b_2 = 302.757865$

$b_3 = 352.018498$

$b_4 = 21.821899$

$b_5 = 48.196927$

$b_6 = 482.485984$

$b_7 = 1114.978885$

$b_8 = 449.690326$

The average stopping power $\overline{\Delta}$ is given by the Bethe Equation as [27]:

$$\overline{\Delta} = \frac{4\pi N_o z^2 e^4 Z\rho}{M_e c^2 \beta^2 A}\left\{\ln \frac{2M_e c^2 \beta^2}{I_{adj}(1-\beta^2)\sqrt{1 + \frac{2M_e}{M_p\sqrt{1-\beta^2}} + \left(\frac{M_e}{M_p}\right)^2}} - \beta^2 - \frac{\Sigma_i C_i}{Z} - \frac{\delta}{2}\right\} \qquad \text{(E-8)}$$

where

ρ = density of the material

z = nuclear charge of the particle

c = velocity of light in a vacuum

e = electronic charge in electrostatic units (ESU)

M_e = rest mass of the electron

A = the atomic weight of the stopping material

N_o = Avogadro's Number

Z = atomic number of the stopping material

I_{adj} = the adjusted ionization potential

β = ratio of the incident particle velocity to the velocity of light

$\Sigma_i C_i$ = the sum of the effects of shell corrections on stopping power

δ = the polarization effect correction term

M_p = proton rest mass

The substitution of $r_o = e^2/M_e C^2$, where r_o is the classical electron radius, provides a useful change of variables in the evaluation of equation (E-8). For a particle of energy E/nucleon, β is given by:

$$\beta = \sqrt{1 - \left(\frac{1}{1 + E/M_p c^2}\right)^2}$$

Given the incident particle's energy and length of trajectory through the glass, the PDF of the energy loss may be computed using equation (E-1). Thus, the stochastic variation of energy loss, or straggling, may be introduced into the Monte Carlo simulation by generating random energy losses from this distribution.

However, these computations were too time prohibitive to evaluate for each simulated charged particle strike. It was thus decided to generate a family of these distributions as a function of charged particle energy, external to the photon noise simulation. Hence, the energy loss for each charged particle striking the PMT window could be quickly obtained from this family of distributions using numerical methods.

The pertinent parameters in the energy loss distribution are pertinent to protons passing through silicon glass:

$\epsilon_1 = 1$ MeV	cutoff energy
$z = 1$	nuclear charge of a proton
$\rho = 2.33$ gr/cm^3	density of silicon
$Z = 14$	atomic number of silicon
$I_{adj} = 170$ eV	ionizing potential of silicon [27]
$M_p = 1.67 \times 10^{-24}$ grams	proton rest mass

$M_E = 9.11 \times 10^{-28}$ grams	electron rest mass
$N_o = 6.02 \times 10^{23}$	Avogadro's number
$r = 2.82 \times 10^{-13}$ cm	classical electron radius.

The last two terms in the Bethe equation limit the stopping power for very high energies and may be set to zero in the present application because the cutoff energy ϵ_1 effectively provides the same limiting function. For a detailed discussion of these terms, see Janni [27] and Sternheimer [28].

With these initial conditions set and $\bar{\Delta}$ and β computed, the integrand in equation (E-1) may now be examined.

The importance of making a careful examination of this surface is two-fold. First a suitable range for the energy loss must be determined so that the density function is zero for $\Delta < \Delta_1$ and also for $\Delta > \Delta_2$, where Δ_1 and Δ_2 are two energies for which energies below Δ_1 or above Δ_2 occur with negligible probabilities. Secondly, the upper limit of integration (the lower limit is always zero) must be chosen so that the PDF is smooth and that increasing the upper limit of integration provides no significant contribution to the integral. Unusual waves and negative values in the PDF are indications that this upper limit needs to be increased.

The energy loss axis is constructed as 65 evenly spaced points between 0.5 and 4.5 (units are in MeV). These limits were chosen as discussed above and will vary with both charge particle type and absorber material. Thirty was found to be suitable as the upper limit of integration. The cutoff energy ϵ_1 was determined to be 1 MeV [29].

The integrand in equation (E-1) is illustrated in Figure E-1 where the variable of integration u is in the u-direction and the energy loss Δ in the Δ-direction. Surfaces of this type proved to be invaluable in choosing the range of Δ and u for various particles and energies.

Performing the numerical integration of the surface yields the desired PDF given in Figure E-2 with its numerical values given in Table E-1.

Vavilov's distribution may be obtained by setting $\epsilon_1 = \epsilon_{max}$ in Equations (E-1) through (E-8).

Figure E-3 compares Vavilov's distribution with Watts' restricted energy loss distribution.

To implement the stochastic behavior of energy transfers into the photon noise model, a family of these distributions was evaluated for proton energies ranging from 700 MeV to 10^5 MeV. This is depicted as an energy surface in Figure E-4, where the E-axis represents proton energy ($\log_{10}$) and the Δ-axis represents deposited energy ($\log_{10}$), i.e., $\log_{10}$ (column labeled Δ in Table E-1).

To implement this into the Monte Carlo simulation, a random proton energy E′ is generated for each proton striking the PMT window. Referring to Figure E-4, the resultant PDF for energy transfer Δ, denoted by $f(\Delta;E')$, is seen to be the intersection of the Δ-Z plane with the surface at $E = E'$.

To obtain the desired energy transfer Δ, the equation

$$\int_0^{\Delta} f(\Delta;E')\, d\Delta = U$$

is solved in terms of Δ, where U is a standard uniform random number. This gives Δ as an energy transfer randomly distributed according to Watts' restricted energy loss distribution.

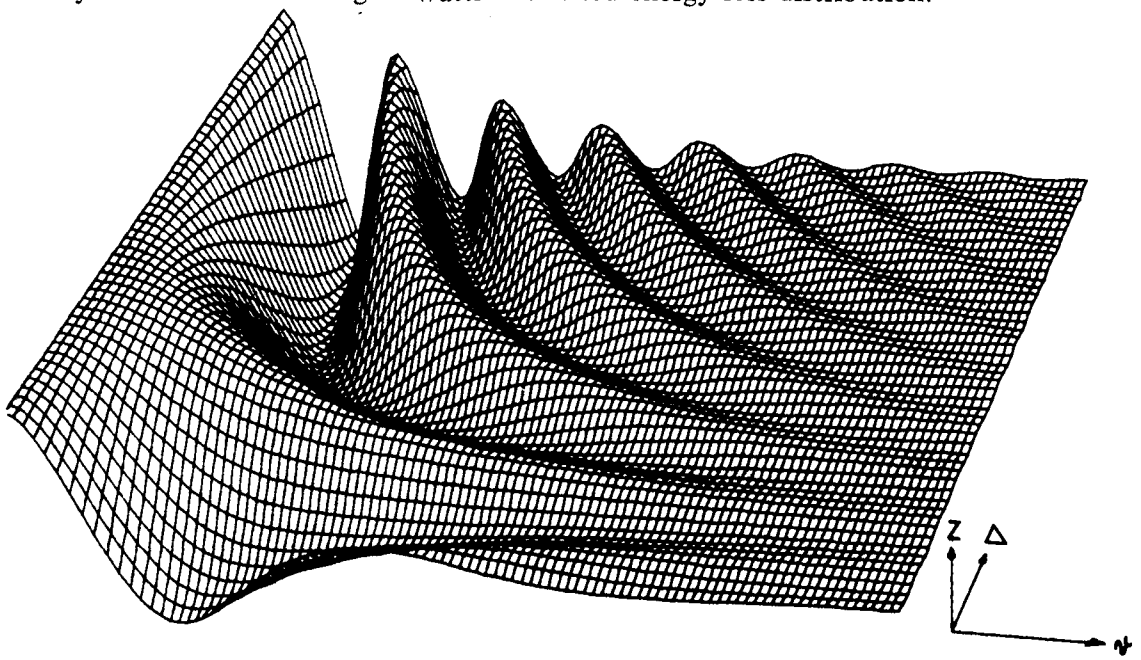

Figure E-1. Integrand of restricted energy loss distribution [equation (E-1)] for 1 BeV proton through 1 cm of silicon glass.

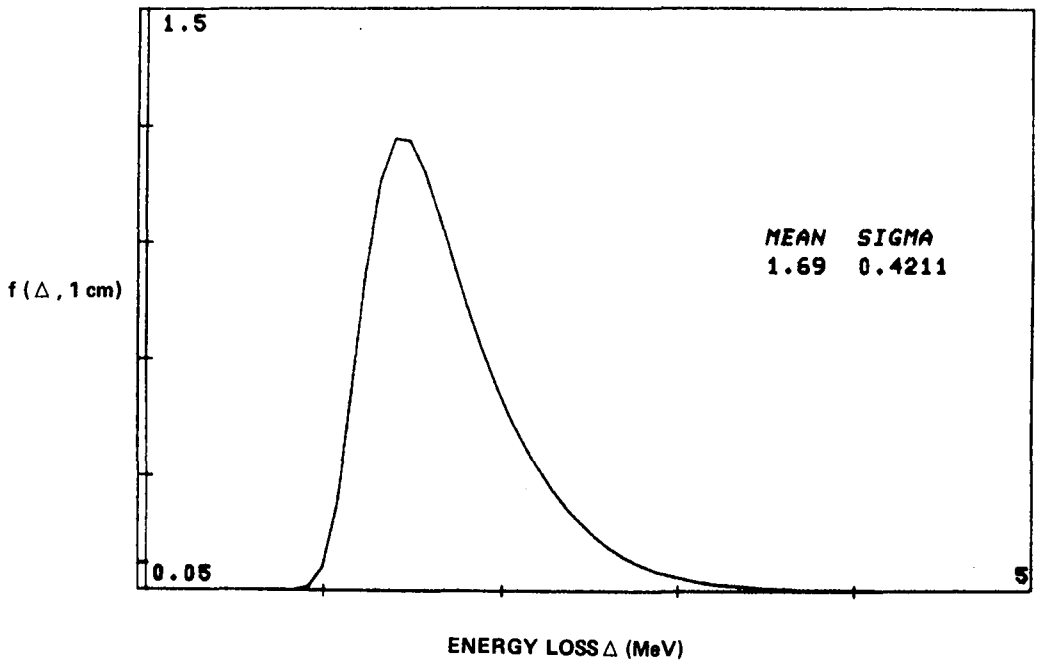

Figure E-2. Restricted energy loss distribution for 1 BeV proton through 1 cm silicon glass.

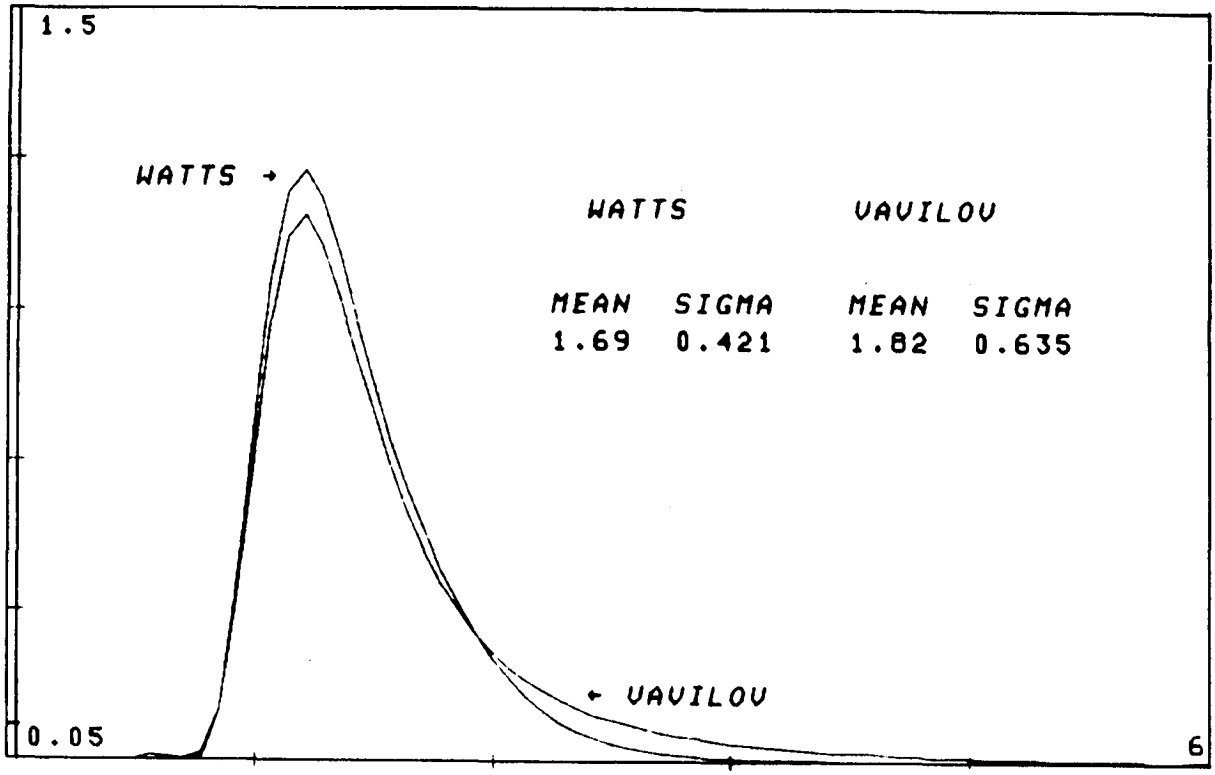

Figure E-3. Vavilov's distribution (set ϵ_1 to ϵ_{max} = 3.3 MeV) versus Watts' restricted energy loss distribution (ϵ_1 = 1 MeV) for proton with incident energy of 1 Bev through 1 cm of silicon glass.

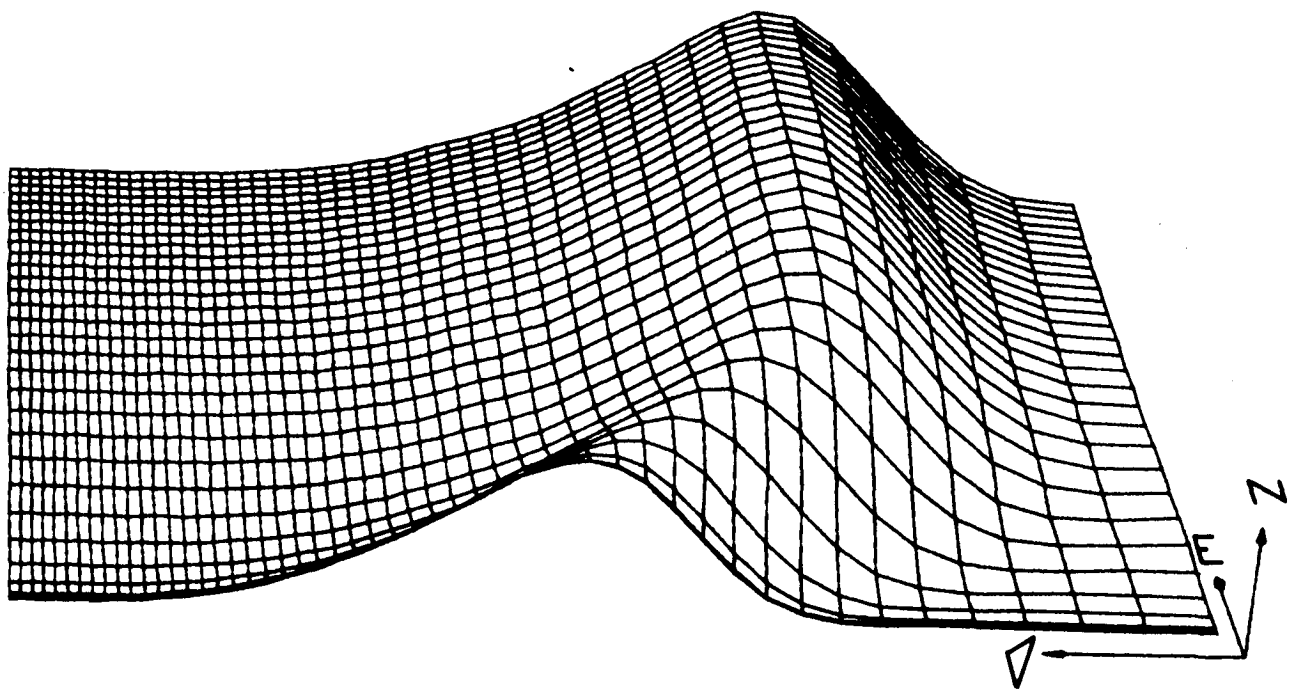

Figure E-4. Family of energy loss PDF's for protons of energy E through 1 cm of silicon glass.

TABLE E-1.

Δ (MEV)	f(Δ; 1 cm)	Δ (MEV)	f(Δ, 1 cm)
0.5625	0.0000	2.5625	0.1291
0.6250	0.0001	2.6250	0.1076
0.6875	0.0000	2.6875	0.0894
0.7500	0.0000	2.7500	0.0740
0.8125	0.0002	2.8125	0.0611
0.8750	0.0023	2.8750	0.0503
0.9375	0.0173	2.9375	0.0413
1.000	0.0737	3.0000	0.0339
1.0625	0.2030	3.0625	0.0277
1.1250	0.4081	3.1250	0.0226
1.1875	0.6521	3.1875	0.0183
1.2500	0.8802	3.2500	0.0148
1.3125	1.0508	3.3125	0.0119
1.3750	1.1474	3.3750	0.0096
1.4375	1.1744	3.4375	0.0077
1.5000	1.1469	3.5000	0.0062
1.5625	1.0834	3.5625	0.0049
1.6250	0.9995	3.6250	0.0039
1.6875	0.9069	3.6875	0.0031
1.7500	0.8137	3.7500	0.0025
1.8125	0.7249	3.8125	0.0019
1.8750	0.6427	3.8750	0.0015
1.9375	0.5684	3.9375	0.0012
2.0000	0.5020	4.0000	0.0009
2.0625	0.4426	4.0625	0.0007
2.1250	0.3888	4.1250	0.0006
2.1875	0.3398	4.1875	0.0005
2.2500	0.2948	4.2500	0.0003
2.3125	0.2536	4.3125	0.0003
2.3750	0.2164	4.3750	0.0002
2.4375	0.1834	4.4375	0.0002
2.5000	0.1543	4.5000	0.0001

APPENDIX F

APL COMPUTER PROGRAM

The following set of APL (a programming language) functions constitute the simulation model. The function HITS on p. 51 is the main program, calling all the others with NHT the number of hits desired. The function HTIC on p. 53 contains the values of most of the model parameters. Any time a function name ends with a Δ it contains a line-by-line commentary on the function of the same name without the Δ. Some functions have commentary within.

```
     ∇ A←S ATAN C
[1]    A←(¯2○C÷((S*2)+C*2)*0.5)×S÷|S
[2]    ⍝
[3]    ⍝ 4 QUADRANT ARC TANGENT
     ∇

     ∇ Y←BC U;Y1;Y2;Y3;UU
[1]    Y1←EL+⊛(U<0.01)/U
[2]    Y2←EL+(⊛UU)+SUM1 UU←((0.01≤U)∧(U≤1))/U
[3]    Y3←((1○UU)×BG UU)-(2○UU)×BH UU←((1<U)∧(U≤50))/U
[4]    →0;Y←Y1,Y2,Y3,(1○UU)÷UU←(U>50)/U
[5]    ⍝
[6]    ⍝  EQ.E4.....APPROXIMATION TO COSINE INTEGRAL
     ∇

     ∇ R←KE BETHE Z;C;MEVFERG;A;ZM;RHO;IZ;MPCS;S;K1;K2;K3
[1]    ⍝.............KE-ENERGY/NUCLEON OF CHARGED PARTICLE (MEV)
[2]    ⍝.............Z-CHARGED PARTICLE CHARGE NUMBER
[3]    C←2.99792458E10⍝....VELOCITY OF LIGHT IN VACUUM--CM/SEC
[4]    MEVFERG←÷1.6021917E 6⍝MEV FROM ERG'S
[5]    MP←1.672614E¯24⍝....PROTON REST MASS GRAMS
[6]    ME←9.109558E¯28⍝....ELECTRON REST MASS GRAMS
[7]    N0←6.022169E23⍝.....AVOGADROS NUMBER--ATOMS/MOLE
[8]    R0←2.82E¯13⍝........CLASSICAL ELECTRON RADIUS-- CM
[9]    A←28.1⍝.............ATOMIC WEIGHT OF SILICON
[10]   ZM←14⍝..............ATOMIC NUMBER OF SILICON
[11]   RHO←2.33⍝...........DENSITY OF SILCON  GRAMS/CM
[12]   IZ←0.00017⍝.........IONIZING POTENTIAL OF SILICON-MEV
[13]   MPCS←MEVFERG×MP×C×C⍝ PROTON REST ENERGY--MEV
[14]   MECS←MEVFERG×ME×C×C⍝ ELECTRON REST ENERGY--MEV
[15]   B←(1-(1+KE÷MPCS)*¯2)*0.5⍝ RATIO OF PARTICLE'S VEL. TO C
[16]   S←1-B×B
[17]   K1←4×○N0×MECS×R0×R0×ZM×Z×Z
[18]   K2←(1+((ME÷MP)*2)+(2×ME÷MP×S*0.5))*0.5
[19]   K3←2×MECS×B×B÷IZ×S
[20]   R←(K1÷B×B×A)×((-B×B)+⊛K3÷K2)
[21]   ⍝
[22]   ⍝  THE BETHE EQUATION----MEV/CM/GM×GM
     ∇
```

```
     ∇ Y←BG U;AA;NUM;DEN
[1]    AA←38.027264 265.187033 335.67732 38.102495 40.021433
       322.624911 570.23628 157.105423
[2]    NUM←+/(((ρU),5)ρ1,4↑AA)×U∘.*8 6 4 2 0
[3]    DEN←+/(((ρU),5)ρ1, 4↑AA)×U∘.*8 6 4 2 0
[4]    →0;Y←NUM÷DEN×U
[5]    ⍝
[6]    ⍝  EQ.E6....G1(U)
     ∇

     ∇ Y←BH U;BB;NUM;DEN
[1]    BB←42.242855 302.757865 352.018498 21.821899 48.196927
       482.485984 1114.978885 449.690326
[2]    NUM←+/(((ρU),5)ρ1,4↑BB)×U∘.*8 6 4 2 0
[3]    DEN←+/(((ρU),5)ρ1,¯4↑BB)×U∘.*8 6 4 2 0
[4]    →0;Y←NUM÷DEN×U×U
[5]    ⍝
[6]    ⍝  EQ.E7.....G2(U)
     ∇

     ∇ Y←BS U;Y1;Y2;Y3;UU
[1]    Y1←(U<0.01)/U
[2]    Y2←SUM2((0.01≤U)∧(U≤1))/U
[3]    Y3←(○0.5)-((2○UU)×BG UU)+(BH UU)×1○UU←((1<U)∧(U≤50))/U
[4]    →0;Y←Y1,Y2,Y3,(○0.5)-(2○UU)÷UU←(U>50)/U
[5]    ⍝
[6]    ⍝ EQ.E5.....APPROXIMATION TO SINE INTEGRAL
     ∇

     ∇ R←CDFI CDF
[1]    →(FLAG=1)/L1
[2]    →0;R←+/CDF<UNF
[3]    L1:R←⌊0.5+ST+(ST*0.5)×NORM
[4]    ⍝
[5]    ⍝ INVERSE CUMULATIVE DISTRIBUTION FUNCTION
     ∇

     ∇ CR;TR;D;DCR;UVWCR;XYZCR;PR;ZAP
[1]    CNTCR←¯1×(FS=1),FS=0
[2]    CNTCR[1+FS]←((RSS≥SPS XYZHT)∧XYZHT[3]=0)∨(RSS≥SPS UVWHT)∧
       UVWHT[3]=0
[3]    →(BN≤1)/0
[4]    TR←⍉(EUL2 ¯2○DHT[3])+.×EUL3 DHT[2]ATAN DHT[1]
[5]    LM:DCR←TR+.×(EUL3○2×UNF)+.×(EUL1 ¯2○÷BN)+.×0 0 1
[6]    UVWCR←DCR EXITTB XYZCR←XYZHT+ΔXYZHT×UNF
[7]    →(DOPR=0)/L0
[8]    PR←PRCR←PRCR,UVWCR,0;PRCR←PRCR,XYZCR,1
[9]    L0:→(ZAP=1)/L1;CNTCR[1+FS]←CNTCR[1+FS]+ZAP←(RSS≥SPS UVWCR)∧
       UVWCR[3]<0.01
[10]   CNTCR[1+FS]←CNTCR[1+FS]+RF UVWCR;D←DCR
[11]   →(DOPR=0)/L1
[12]   PRCR←PR
[13]   L1:→(0<NCR←NCR-1)/LM
     ∇
```

```
    ∇ CRΔ
[1]   ⍝ DATA IS SAVED SPLIT INTO TOP/BOTTOM AND SIDES, ¯1 OCCUPIE
      S THE NOT USED SPOT
[2]   ⍝ COUNT IF ENTRY OF EXIT POINT OF PARTICLE PATH IN CATHODE
[3]   ⍝ OMIT CERENKOV IF ENERGY TOO LOW
[4]   ⍝ TRANSFORMATION FROM COORD SYS WITH Z-AXIS ALONG MAIN PATH
       TO XYZ COOPD SYS, USING CERENKOV PHASE ANGLE ( 2○÷RN⍵ OF A
      BOUT 47 DEG
[5]   ⍝ GET DIR COS WITH CERENKOV ANGLE AND UNIF AZIMUTH ABOUT MA
      IN PATH
[6]   ⍝ PICK UNIF DISTR ALONG PATH AND GET EXIT POINT
[7]   ⍝ SKIP NEXT LINE FOR NO GRAPHICS
[8]   ⍝ SAVE GRAPHICS DATA
[9]   ⍝ ZAP=1 IF CATHODE HIT, ENDS PATH OF THIS PHOTON BY JUMP TO
       L1
[10]  ⍝ GET COUNT FROM REFLECTIONS AND SAVE
[11]  ⍝ SKIP NEXT LINE IF NO GRAPHICS
[12]  ⍝ SAVE GRAPHICS DATA
[13]  ⍝ REPEAT FROM LM UNTIL NCR=0 (NO OF REMAINING CERENKOV PHOT
      ONS⍵
    ∇

    ∇ R←EUL1 A
[1]   R←3 3⍴(1 0,1○-A,-A,A+○0.5⍵[1 2 2 2 5 4 2 3 5]
[2]   ⍝
[3]   ⍝ EULER ANGLE ROTATION MATRIX ABOUT X-AXIS
    ∇

    ∇ R←EUL2 A
[1]   R←3 3⍴(1 0,1○-A,-A,A+○0.5⍵[5 2 3 2 1 2 4 2 5]
[2]   ⍝
[3]   ⍝ EULER ANGLE ROTATION MATRIX ABOUT Y-AXIS
    ∇


    ∇ R←EUL3 A
[1]   R←3 3⍴(1 0,1○-A,-A,A+○0.5⍵[5 4 2 3 5 2 2 2 1]
[2]   ⍝
[3]   ⍝ EULER ANGLE ROTATION MATRIX ABOUT Z-AXIS
    ∇

    ∇ UVW←H EXITSD XYZ;X;Y;Z;U;V;ΔZ;SC;D2
[1]   X←XYZ[1];Y←XYZ[2];Z←XYZ[3];D2←|DHT[2]
[2]   U←2×RM×DHT[1]×D2÷1-DHT[3]×DHT[3]
[3]   V←(D2×U÷DHT[1])-RM
[4]   ΔZ←DHT[3]×U÷DHT[1]
[5]   →(ΔZ≤HM-Z)/NTS
[6]   →TB;SC←(HM-Z)÷ΔZ;H←HM
[7]   NTS:→(ΔZ≥-Z)/NBS
[8]   SC←-Z÷ΔZ;H←0
[9]   TB:U←SC×U;V←(SC×V+RM⍵-RM
[10]  →0;UVW←U,V,H
[11]  NBS:UVW←U,V,Z+ΔZ
[12]  ⍝
[13]  ⍝ EXIT POINT FOR SIDE ENTERIES
    ∇
```

```
     ∇ UVW←D EXITTB XYZ;A;B;C;SC;ΔXYZ
[1]    H←-(XYZ[3]-HM×D[3]≥0)÷D[3]
[2]    UVW←XYZ+ΔXYZ←D×H
[3]    →(RMS≥SPS UVW)/0
[4]    A←SPS ΔXYZ
[5]    B←-+/(XYZ×ΔXYZ)[1 2]
[6]    SC←(B+((B×B)+(RMS-SPS XYZ)×A)*0.5)÷A
[7]    UVW←XYZ+ΔXYZ←SC×ΔXYZ
[8]    ⍝
[9]    ⍝ EXIT POINT FOR TOP/BOTTOM ENTRY
     ∇

     ∇ FL;D;PR;DFL;ZAP
[1]    CNTFL←¯1×(FS=1),FS=0
[2]    →(0=NFL)/0
[3]    PT:XYZFL←XYZHT+ΔXYZHT×UNF
[4]    DFL←GENDC
[5]    UVWFL←DFL EXITTB XYZFL
[6]    CNTFL[1+FS]←CNTFL[1+FS]+ZAP←(RSS≥SPS UVWFL)∧UVWFL[3]<0.01
[7]    →(DOPR=0)/L0
[8]    PR←PRFL←PRFL,UVWFL,0;PRFL←PRFL,XYZFL,1
[9]    L0:D←DFL;→(ZAP=1)/L1
[10]   CNTFL[1+FS]←CNTFL[1+FS]+RF UVWFL
[11]   →(DOPR=0)/L1
[12]   PRFL←PR
[13]   L1:→(0<NFL←NFL-1)/PT
     ∇

     ∇ FLΔ
[1]    ⍝ SEE COMCR[1]
[2]    ⍝ JUMP OUT FOR NO FL PHOTONS
[3]    ⍝ PICK UNIF DISTR ALONG PATH
[4]    ⍝ GET UNIF DISTR DIR COS
[5]    ⍝ GET EXIT POINT
[6]    ⍝ DETERMINES IF CATHODE IS HIT AND SAVES COUNT
[7]    ⍝ SKIP NEXT LINE FOR NO GRAPHICS
[8]    ⍝ SAVE GRAPHICS DATA
[9]    ⍝ TAKE CARE OF NEXT PHOTON IF CATHODE IS HIT
[10]   ⍝ SAVE FLUORESCENT COUNT
[11]   ⍝ SKIP NEXT LINE FOR NO GRAPHICS
[12]   ⍝ SAVE GRAPHICS DATA
[13]   ⍝ COUNT NLF DOWN BY ONE AND REPEAT FROM PT IF NOT ZERO
     ∇

     ∇ D←GENDC;AZ;S
[1]    D←(((1-S×S)*0.5)×(2○AZ),1○AZ←○2×UNF),S←2×¯0.5+UNF
[2]    ⍝
[3]    ⍝ RANDOMLY DISTRIBUTED DIRECTION COSINES
     ∇
```

```
     ∇ GENKINEN
[1]    →(SAA=1)/L
[2]    ENPN←JFBEV×KEBEV←(1-UNF×(1-CUTOFF*1-GAM1))*÷1-GAM1
[3]    →LL
[4]    L:ENPN←JFMEV×GENLOGNORM 4.7 1⍝ MODEL FOR SAA PROTONS AND A
       LPHA PARTICLES
[5]    LL:BN←N7056×(1-(1+ENPN÷M0C2)*¯2)*0.5
[6]    ⍝
[7]    ⍝ KINETIC ENERGY AND BETA ANGLE
     ∇

     ∇ E←GENLOGNORM PARAM;MU;VAR
[1]    VAR←PARAM[2];MU←PARAM[1]
[2]    E←*MU+(VAR*0.5)×NORM
[3]    ⍝
[4]    ⍝ GENERATES N LOG-NORMAL RANDOM NUMBERS WITH PARAMETERS
[5]    ⍝ MU AND VAR (MU AND VAR ARE THE MEAN AND VARIANCE OF
[6]    ⍝ THE DEFINING NORMAL DISTRIBUTION).
     ∇

     ∇ GENRTRPAV;N;TH;CTH;STHT;CTHT;RT;RP;TT;TP
[1]    N←N7056
[2]    CTH←DMIN+(1-DMIN)×0,0.02×⍳50
[3]    TH←¯2○CTH
[4]    CTHT←(1-STHT×STHT←N×1○TH)*0.5
[5]    RT←RT×RT←(CTHT-N×CTH)÷CTHT+N×CTH⍝  REFLECTION, PARALLEL
[6]    RP←RP×RP←(CTH-N×CTHT)÷CTH+N×CTHT⍝  REFLECTION, PERPENDICULA
       R
[7]    TT←(CTHT÷N×CTH)×TT×TT←2×N×CTH÷CTHT+N×CTH⍝ TRANSMISSION, PER
       PENDICULAR
[8]    TP←(CTHT÷N×CTH)×TP×TP←2×N×CTH÷CTH+N×CTHT⍝ TRANSMISSION, PAR
       ALLEL
[9]    RTRPAV←1↓0.5×RT+RP⍝   AVERAGE OF RT+RP
     ∇

     ∇ Y←G1 U
[1]    →0;Y←(((⍴B),⍴U)⍴(-(2○U)+U×BS U))+(B×B×E1÷E)∘.×(⊛U)-BC U
[2]    ⍝
[3]    ⍝  EQ.E2
     ∇

     ∇ Y←G2 U
[1]    →0;Y←((B×B×E1÷E)∘.×BS U)+((⍴B),⍴U)⍴(1○U)+U×(⊛U)-BC U
[2]    ⍝
[3]    ⍝  EQ.E3
     ∇
```

```
     ∇ HITS NHT;DHT;XYZHT;UVWHT;NCR;NFL
[1]    HTIC
[2]    PRCNTHT←⍳0
[3]    PRLD←PRCNTCR←PRCNTFL←2 0⍴0
[4]    L1:PRHT←PRCR←PRFL←4 0⍴0
[5]    HT
[6]    CR
[7]    FL
[8]    PRCNTCR←PRCNTCR,CNTCR;PRCNTFL←PRCNTFL,CNTFL
[9]    →(0<NHT←NHT-1)/L1
     ∇

     ∇ HITSΔ
[1]    ⍝ INITIALIZATION
[2]    ⍝ SET UP
[3]    ⍝ DATA SAVING
[4]    ⍝ RESET GRAPHICS DATA
[5]    ⍝ GENERATE RANDOM PARTICLE STRIKE PATH
[6]    ⍝ EVALUATE CERENKOV PHOTONS
[7]    ⍝ EVALUATE FLUORESCENT PHOTONS
[8]    ⍝ SAVE CENRENKOV AND FLUORESCENT COUNTS
[9]    ⍝ GO BACK FOR NEXT HIT UNTIL HITCOUNT NHT IS ZERO
     ∇

     ∇ HT;TR;L;ST
[1]    DHT←GENDC
[2]    →(RTB>UNF)/TB
[3]    XYZHT←0,(-RM),HM×UNF;FS←1
[4]    UVWHT←HM EXITSD XYZHT
[5]    PRCNTHT←PRCNTHT,(RSS≥SPS UVWHT)∧UVWHT[3]<0.01
[6]    TR←EUL3○2×UNF
[7]    XYZHT←TR+.×XYZHT
[8]    UVWHT←TR+.×UVWHT
[9]    →CL
[10]   TB:XYZHT←(RM×2×¯0.5+UNF,UNF),HM×DHT[3]<0;FS←0
[11]   →(RMS<SPS XYZHT)/TB
[12]   UVWHT←DHT EXITTB XYZHT
[13]   PRCNTHT←PRCNTHT,((RSS≥SPS UVWHT)∧UVWHT[3]<0.01)∨(RSS≥SPS
       XYZHT)∧XYZHT[3]<0.01
[14]   CL:L←(+/(ΔXYZHT←UVWHT-XYZHT)*2)*0.5
[15]   PRLD←PRLD,L,DHT[3]
[16]   GENKINEN
[17]   →(BN≤1)/L0
[18]   NCR←CDFI POISSON ST←KANCR×L×1-÷BN×BN
[19]   ⍝ L0:NFL←CDFI POISSON ST←KANFL×L×BN BETHE Z
[20]   L0:NFL←CDFI POISSON ST←KANFL×L×WATTSPR ENPN×MEVFJ
[21]   →(DOPR=0)/0;⍝ 'NCR,NFL=';NCR,NFL
[22]   PRHT←PRHT,UVWHT,0;PRHT←PRHT,XYZHT,1
     ∇
```

```
    ∇ HT∆
[1]   ⍝ PARTICLE PATH DIR COS, DHT[3]>0 IS UPWARD HIT
[2]   ⍝ GO TO TB IF TOP/BOTTOM HIT
[3]   ⍝ GET HIGHT OF SIDE ENTRY, SET SIDE FLAG
[4]   ⍝ GET EXIT POINT FOR SIDE ENTRY
[5]   ⍝ SAVE MAIN STRIKE, 1 FOR PHOTOCATHODE HIT
[6]   ⍝ TRANSFORMATION ABOUT Z AXIS WITH RANDOM ANGLE
[7]   ⍝ TRANSFORM ENTRY POINT
[8]   ⍝ TRANSFORM EXIT POINT
[9]   ⍝ GO TO CL
[10]  ⍝ PICK TOP (DHT[3]>0) OR BOTTOM POINT IN A 2×RM SQUARE; RES
      ET SIDE FLAG
[11]  ⍝ REDO POINT IF OUTSIDE RM RADIUS CIRCLE
[12]  ⍝ GET EXIT POINT
[13]  ⍝ SAVE A 1 IF ENTRY OR EXIT POINT HIT PHOTOCATHODE, OTHERWI
      SE SAVE 0
[14]  ⍝ GET PATHLENGTH
[15]  ⍝ SAVE PATHLENGHT AND DHT[3] (UPHIT DHT[3]>0)
[16]  ⍝ GENREATE KINETIC ENERGY
[17]  ⍝ SKIP CERENKOV PHOTON NCR GENERATION IF ENERGY TOO LOW
[18]  ⍝ GET CERENKOV PHOTON NO WITH POISSON AVERAGE
[19]  ⍝ GET FLUORESCENT PHOTON NO WITH POISSON AVERAGE (FOR LOW Z
      )
[20]  ⍝ GET FLUORESCENT PHOTON NO WITH POISSON AVERAGE (FOR HIGH
      Z)
[21]  ⍝ SKIP NEXT LINE IF NO GRAPHICS
[22]  ⍝ SAVE GRAPHICS DATA
    ∇
```

```
    ∇ HTIC
[1]   Z←1⍝ PARTICLE CHARGE NUMBER
[2]   DOPR←1⍝ DOPR=1 FOR GRAPHICS (OVERFLOWS WORKSPACE CAPACITY F
      OR LARGE Z)
[3]   SAA←0⍝ SAA=1 RESULTS IN SAA CHARGED PARTICLES;0 IMPLIES COS
      MIC RAYS
[4]   ⍝ ******** DEDX2 NEEDED FOR SAA=1, CHANGE IN ∇HT∇ NEEDED **
      *****
[5]   N7056←1.487⍝ REFR INDEX
[6]   RHO←2.33⍝  DENSITY OF GLASS  GRAMS/ML
[7]   A←28.086⍝  ATOMIC WEIGHT OF SILICON
[8]   ZM←14⍝   ATOMIC NUMBER OF SILICON
[9]   IZ←170⍝  IONIZING POTENTIAL OF SILICON--MEV
[10]  R0←2.81794E 13⍝  CLASSICAL ELECTRON RADIUS--CM
[11]  N0←6.02486E23⍝  AVOGAGROS NUMBER ATOMS/MOLE
[12]  MP←1.67261E¯24⍝  PROTON REST MASS--GRAMS
[13]  ME←9.10956E¯28⍝  ELECTRON REST MASS--GRAMS
[14]  MCSQ←0.51097⍝  ONE RYDBERG
[15]  DMIN←(1-(÷N7056)*2)*0.5⍝  COS OF TOTAL REFLECTION ANGLE
[16]  DMINM←-DMIN;KRT←50÷1-DMIN;GENRTRPAV
[17]  ⍝ SID←RFD×0⍝ SIGMA OF REFLECTION VARIATION
[18]  KTR←0.000379⍝ TRANSMISSION LOSS, ABSORPTION
[19]  L0:→L0+Z
[20]  →L1;GAM1←2.7⍝  Z=1 PROTON  GAM1 IS INTEGRAL FLUX OF PROTON
      INTENSITIES
[21]  →L1;GAM1←2.7⍝  Z=2 ALPHA NASA SP-243,P 0.135
[22]  →L1;GAM1←2.56⍝ Z=3 LITHIUM
[23]  →L1;GAM1←2.56⍝ Z=4 BERYLLIUM
[24]  →L1;GAM1←2.35⍝ Z=5 BORON  ASTRO. JOURNAL,218:269-285, 1977
      NOV 15
[25]  →L1;GAM1←2.76⍝ Z=6 CARBON
[26]  →L1;GAM1←3.07⍝ Z=7 NITROGEN
[27]  →L1;GAM1←2.67⍝ Z=8 OXYGEN
[28]  →L1;GAM1←3.01⍝ Z=9 FLUORINE
[29]  →L1;GAM1←2.88⍝ Z=10 NEON
[30]  L1:MOC2←1.673E¯27×299792458*2
[31]  CUTOFF←100⍝   CUTOFF FOR HIGH ENERGIES-- UNITS IN BEV
[32]  RM←9.5⍝ PMT WINDOW RADIUS IN MM
[33]  RS←1.5⍝ PHOTO CATHODE RADIUS IN MM
[34]  HM←1.5⍝ PMT WINDOW HEIGHT IN MM
[35]  RR←RM-1⍝ RING RADIUS IN MM, 1 AS MEASURED BY US
[36]  KLAM←244⍝ 7056 GLASS WAVELENGTH INTEGRAL
[37]  RTB←RM÷RM+HM
[38]  RMS←RM×RM;RSS←RS×RS;RRS←RR×RR
[39]  KANCR←(Z×Z×○2÷137.03602)×KLAM⍝ FIRST FACTOR IN EQU. FOR CER
      ENKOV RADIATION (TN D-8147)
[40]  KANFL←2×8⍝  FACTOR OF TWO IMPLIES 4 PI STERADIANS (PERS. CO
      NVER. WITH WALTER VIEHMANN)
[41]  ⍝ FACTOR OF 8 FROM TABLE 1 (TRIALKALI 7056) OF TN D-8147
[42]  CIRCT←RS×CIRC
[43]  JFBEV←1.60219E¯10⍝ JOULE FROM BILLION ELECTRON VOLTS
[44]  JFMEV←JFBEV÷1000
[45]  MEVFJ←÷JFMEV
    ∇
```

```
     ∇ O←V INTEGRATE T
[1]    O←(V[2]-V[1])×(-0.5×((1↓ρT)ρ,T)+(1↓ρT)ρ,⍬[1]T←⍉T)++/T←T
[2]    ⍝
[3]    ⍝  INTEGRATES A MATRIX OR VECTOR WHERE T=F(V)
     ∇

     ∇ Y←XY INTPOL1 X;NX;NY;N1;N2;X1;X2;Y1;Y2
[1]    →((XY[1;1]>⌊/X)∨(⌈/X)≥¯1↑XY[1;])/E
[2]    N2←1+N1←+/(⍉(NY,NX)ρX)≥((NX←ρX),NY←(ρXY)[2])ρXY[1;]
[3]    X1←XY[1;N1];X2←XY[1;N2];Y1←XY[2;N1];Y2←XY[2;N2]
[4]    Y←Y1+(Y2-Y1)×(X-X1)÷X2-X1
[5]    →0
[6]    E:'X OUTSIDE RANGE'
[7]    ⍝ LINEAR INTERPOLATION
[8]    ⍝ XY[1;] MUST INCREASE MONOTONICALLY,
[9]    ⍝ BUT DOES NOT HAVE TO BE EVENLY SPACED
     ∇


     ∇ R←NORM
[1]    R←((¯2×⍟UNF)*0.5)×2○2×UNF
[2]    ⍝
[3]    ⍝ NORMAL DISTRIBUTION BASED ON THE POLAR METHOD
     ∇

     ∇ CDF←POISSON ST;P0;P;K
[1]    →(ST>177)/L1
[2]    FLAG←0
[3]    CDF←P0←*-ST
[4]    K←P←1
[5]    L0:P←P×ST÷K
[6]    CDF←CDF,(¯1↑CDF)+P×P0
[7]    K←K+1
[8]    →(0.9999>¯1↑CDF)/L0
[9]    →0
[10]   L1:FLAG←1;CDF←⍳0
[11]   ⍝
[12]   ⍝ GENERATES POISSON DISTRIBUTION WITH MEAN ST
     ∇
```

```
    ∇ NN PROFAMILY UE;LM;E;P;C;D;Δ;KE;K;T;U;R
[1]   KEV←PROTONKEV;N←NN[1];M←NN[2];K←1
[2]   V←N PTS 0.6 4;Δ←U[2]-U[1];U←M PTS 1E¯10,UE;R←(N,ρKEV)ρ0
[3]   L:LM←KE BETHE Z←1;I←ρKE←¯2↑(2×K)↑KEV;MM←¯2↑(2×K)↑ιρKEV
[4]   T←○2×N0×MECS×R0×R0×Z×Z÷B×B
[5]   E←2×MECS×B×B÷(1-B×B)×1+(2×S)+S×S←ME÷MP
[6]   P←T÷E1←1;EL←0.5772156649
[7]   C←(÷○E1)××P×1+E1×B×B×EL÷E
[8]   D←(((V∘.×Iρ1)-(N,I)ρLM)÷(N,I)ρE1)-(N,I)ρP×(B×B)+1+(⊛E1÷E)-
      EL
[9]   R[;MM]←((N,I)ρC)×INT((N,I,M)ρ(*(P∘.×Mρ1)×G1 U))×2○(D∘.×U)+(
      N,I,M)ρ(P∘.×Mρ1)×G2 U
[10]  →(((ρKEV)÷2)≥K←K+1)/L;K
[11]  PROTONFAMILY←R÷((1↑ρR)ρ1)∘.×V INTEGRATE⍉R
[12]  →0
[13]  ⍝ M IS THE NO. OF PARTITIONS OF THE VARIABLE U OF
[14]  ⍝ INTEGRATION; N IS THE NO OF FREQ. PTS. FOR EACH
[15]  ⍝ OF THE RESULTANT DISTRIBUTIONS; PROTONKEV IS THE
[16]  ⍝ VECTOR ENERGIES PER NUCLEON OF THE CHARGED PARTICLE;
[17]  ⍝ R IS THE MATRIX WHICH CONTAINS THE FAMILY OF DENSITY
[18]  ⍝ FUNCTIONS; UE IS THE UPPER LIMIT OF INTEGRATION;
[19]  ⍝ Δ IS THE INTEGRATION STEP SIZE; B IS THE RATIO OF
[20]  ⍝ THE PROTON'S VELOCITY TO LIGHT, I.E., B=V÷C;  KEV IS
[21]  ⍝ PRIMARY PARTICLE ENERGY IN MEV/NUCLEON;  Z IS PRIMARY
[22]  ⍝ CHARGE NO.; N0 IS AVOGADRO'S NO.; R0 IS CLASSILAL
[23]  ⍝ ELECTRON RADIUS; ME IS ELECTRON REST MASS; MP IS
[24]  ⍝ PROTON MASS (Z=1); E IS MAX. POSSIBLE ENERGY
[25]  ⍝ TRANSFER; EL IS EULER'S CONSTANT; T IS ZETA
[26]  ⍝ DEFINED IN EQ. E1; E1 IS DELTA RAY CUTOFF ENERGY.
[27]  ⍝
[28]  ⍝
[29]  ⍝ PROFAMILY PRODUCES A FAMILY OF RESTRICTED ENERGY LOSS
[30]  ⍝ DISTRIBUTIONS.  EACH GENERATED DISTRIBUTION CORRES-
[31]  ⍝ PONDS TO AN ENERGY DEFINED EXTERNALLY BY THE VECTOR
[32]  ⍝ PROTONKEV WHICH SHOULD CONTAIN AN EVEN NUMBER OF
[33]  ⍝ ELEMENTS.
    ∇

    ∇ CNT←RF UVW;XYZ;ZAP;NCO
[1]   CNT←NCO←0
[2]   TBSD:→((UVW[3]≠0)∧UVW[3]≠HM)/SD
[3]   →(DMIN≥|D[3])/TR⍝ TOTAL REFLECTION
[4]   →(RTRPAV[⌈KRT×DMINM+|D[3]]≤UNF)/0⍝ TRANSMISSION
[5]   TR:→L0;D←1 1 ¯1×D
[6]   SD:NCO←NCO+1
[7]   AL←UVW[2]ATAN UVW[1]
[8]   D←(EUL3 AL)+.×D
[9]   →(DMIN<D[1])/0⍝ TRANSMISSION
[10]  →((|D[2])≥D[1]×RS÷(RMS-RSS)*0.5)/0⍝ SIDE REFLECTION MISSES
      PHOTOCATHODE
[11]  D←(EUL3-AL)+.×D×¯1 1 1
[12]  L0:UVW←D EXITTB XYZ←UVW
[13]  CNT←CNT+ZAP←(RSS≥SPS UVW)∧UVW[3]<0.01
[14]  →((UVW[3]<0.01)∨XYZ[3]<0.01)/0⍝ NO BOTTOM REFLECTIONS
[15]  →(DOPR=0)/L1
[16]  PR←PR,UVW,0
[17]  L1:→(UNF>1-KTR×(+/(UVW-XYZ)*2)*0.5)/0⍝ TRANSMISSION LOSS
[18]  →((ZAP=0)∧NCO<10)/TBSD
    ∇
```

```
     ∇ RF∆
[1]    ⍝ SET COUNT AND MAX SIDE STRIKES TO ZERO
[2]    ⍝ IF NOT ON TOP OR BOTTOM, GO TO SD
[3]    ⍝ IF TOTAL REFLECTION, GO TO TR
[4]    ⍝ JUMP OUT IF TRANSMISSION (UNIF PICK FROM TRANSMISSION CUR
       VE)
[5]    ⍝ RFLECT AND GO TO L0
[6]    ⍝ INCR SIDE STRIKE NO
[7]    ⍝ GET SIDE INCIDENCE ANGLE
[8]    ⍝ TRANSFORM D WITH SIDE INCID ANGLE
[9]    ⍝ JUMP OUT IF TRANSMISSION
[10]   ⍝ JUMP OUT IF SIDE REFLECTION MISSES CATHODE
[11]   ⍝ REFLECT AND TRANSFORM BACK TO XYZ COORD SYS
[12]   ⍝ SET PREVIOUS 'EXIT' POINT TO 'ENTRANCE' POINT AND GET NEW
        'EXIT' POINT
[13]   ⍝ CHECK FOR CATHODE HIT AND SAVE COUNT
[14]   ⍝ JUMP OUT IF NO BOTTOM REFLECTIONS
[15]   ⍝ SKIP NEXT LINE IF NO GRAPHICS
[16]   ⍝ SAVE GRAPHICS DATA
[17]   ⍝ JUMP OUT IF TRANSMISSION LOSS ALONG PHOTON PATH
[18]   ⍝ REPEAT FROM TBSD IF NO STRIKE AND LESS THAN 10 SIDE REFLE
       CTIONS
     ∇

     ∇ R←AXIS SMOOTH S
[1]    R←0⌈S
[2]    R←R÷((1↑⍴R)⍴1)∘.×AXIS INTEGRATE R
[3]    ⍝
[4]    ⍝  SMOOTHES FAMILY OF VAVILOV DISTRIBUTIONS
     ∇

     ∇ R←SPS I
[1]    R←+/(I×I)[1 2]
     ∇

     ∇ Y←SUM1 U;NUM;DEN;J
[1]    NUM←(U∘.*2×J)×((⍴U),⍴J)⍴¯1*2|J←⍳25
[2]    DEN←((⍴U),⍴J)⍴(!2×J)×2×J
[3]    →0;Y←+/NUM÷DEN
[4]    ⍝
[5]    ⍝  INFINITE SERIES WHICH APPEARS IN THE COSINE INTEGRAL
[6]    ⍝  APPROXIMATION IN EQ.E4
     ∇

     ∇ Y←SUM2 U;NUM;DEN;J
[1]    NUM←(U∘.*1+2×J)×((⍴U),⍴J)⍴¯1*2|J←¯1+⍳25
[2]    DEN←((⍴U),⍴J)⍴(!1+2×J)×1+2×J
[3]    →0;Y←+/NUM÷DEN
[4]    ⍝
[5]    ⍝  INFINITE SERIES WHICH APPEARS IN THE SINE INTEGRAL
[6]    ⍝  APROXIMATION IN EQ.E5
     ∇
```

```
    ∇ U←UNF
[1]   U←1E¯9×¯1+?1000000001
[2]   ⍝
[3]   ⍝ STANDARD UNIFORM RANDOM NUMBERS
    ∇


    ∇ NN VAVPROTON UE;T;E;P;C;D;S;KE;U;PROTONSUR;LM
[1]   I←⍴KE←1000;N←NN[1];M←NN[2]⍝ ENERGY IS IN MEV
[2]   LM←KE BETHE Z←1
[3]   V←N PTS 0.5 4.5;U←M PTS 1E¯10,UE
[4]   T←○2×N0×MECS×R0×R0×Z×Z÷B×B
[5]   E←2×MECS×B×B÷(1-B×B)×1+(2×S)+S×S←ME÷MP
[6]   P←T÷E1←1;EL←0.5772156649
[7]   C←(÷○E1)×*P×1+E1×B×B×EL÷E
[8]   D←(((V∘.×I⍴1)-(N,I)⍴LM)÷(N,I)⍴E1)-(N,I)⍴P×(B×B)+1+(⊛E1÷E)-
      EL
[9]   PROTONSUR←((N,I,M)⍴C∘.×M⍴1)×((N,I,M)⍴(*(P∘.×M⍴1)×G1 U))×2○(
      D∘.×U)+(N,I,M)⍴(P∘.×M⍴1)×G2 U
[10]  ⍝
[11]  ⍝  PRODUCES THE FUNCTION F(X,Δ) BEFORE INTEGRATION
[12]  ⍝
[13]  PDF←V SMOOTH U INTEGRATE PROTONSUR
    ∇

    ∇ DEDX←WATTSPR E;U;I;J;Z
[1]   I←¯1 0 1 2++/EAX≤E
[2]   U←UNF;J←1;Z←⍳0
[3]   R←2,⍴DEAXPR
[4]   L:Z←Z,(R⍴IVAVPR[;I[J]],DEAXPP)INTPOL1 U
[5]   →(4≥J←J+1)/L
[6]   DEDX←0.1×RHO×(2 4⍴EAX[I],Z)INTPOL1 E⍝  MEV/GR2/CM TO MEV/MM
[7]   ⍝
[8]   ⍝ ENERGY DEPOSITION DEDX GIVEN PARTICLE ENERGY E
    ∇
```

REFERENCES

1. Allen, William H. (ed.): Dictionary of Technical Terms for Aerospace Use. Scientific and Technical Information Division, NASA, 1975.

2. Stassinopoulos, E. G.: The ST Environment: Expected Charged Particle Radiation Levels. NASA X-601-78-30, Table 19, October 1978.

3. Juliusson, E. and Meyer, P.: A Measurement of Abundances of VVH (very, very heavy) Nuclei Above 0.6 GeV Per Nucleon. Astrophysical Journal, Vol. 201, 1975, pp. 76-81.

4. Caldwell, John H.: Charge Composition and Energy Spectra of Cosmic-Ray Nuclei at Energies Above 5 GeV per Nucleon. Astrophysical Journal, Vol. 218, November 15, 1977, pp. 269-285.

5. Parnell, Thomas A., Chief, High Energy Physics Branch, Astrophysics Division, Space Science Lab., MSFC, Huntsville, AL, personal communication, 1982.

6. Janossy, L.: Cosmic Rays. Oxford Univ. Press, 1950.

7. Watts, J. W., Burrell, M. O., and Wright, J. T.: Charged Particle Radiation Environment for the LST. NASA TM X-64858, May 1974.

8. Good, Irving J., University Distinguished Professor of Statistics, Virginia Polytechnic Inst. and State Univ., Blacksburg, VA, personal communication, 1982.

9. Noll, R. B. and McElroy, M. B.: The Earth's Trapped Radiation Belts. NASA SP-8116, March 1975.

10. EMI Industrial Electronics: Catalog, 1979.

11. EMR Photoelectric: Multiplier Phototube Catalog, 1975.

12. Viehmann, W. and Eubanks, A. G.: Noise Limitations of Multiplier Phototubes in the Radiation Environment of Space. NASA TN D-8147, March 1976.

13. Viehmann, W.; et al.: Photomultiplier Window Materials Under Electron Irradiation: Fluorescence and Phosphorescence. Applied Optics, Vol. 14, No. 9, September 1975.

14. Hecht, Eugen, and Zajac, Alfred: Optics. Addison-Wesley Pub. Co., 1975, pp. 74-80.

15. Teich, M. C.: Role of the Doubly Stochastic Neyman Type-A and Thomas Counting Distributions in Photon Detection. Applied Optics, Vol. 20, No. 14, July 1981.

16. Teich, M. C. and Saleh, B. E.: Fluctuation Properties of Multiplied-Poisson Light: Measurement of the Photon-Counting Distribution for Radioluminescence Radiation from Glass. The American Physical Society, 1981.

17. Saleh, B. E., Tavolacci, J. T., and Teich, M. C.: Discrimination of Shot-Noise-Driven Poisson Processes by External Dead Time: Application to Radioluminescence from Glass. IEEE Journal of Quantum Electronics, Vol. QE-17, No. 12, December 1981.

18. Saleh, B. E. and Teich, M. C.: Multiplied-Poisson Noise in Pulse, Particle, and Photon Detection. Proc. of the IEEE, Vol. 70, No. 3, March 1982.

19. Lehmer, D. H.: Proc. 2nd Symposium on Large-Scale Digital Computing Machinery. Cambridge, Harvard Univ. Press, 1591, pp. 141-146.

20. Marsaglia, G.: The Structure of Linear Congruential Sequences; Applications of Number Theory to Numerical Analysis. S. K. Zaremba (ed.), Academic Press, 1972.

21. Carroll, Stan N.: Pseudo-Random Number Generator for the Sigma V Computer. NASA TM-82516, February 1983.

22. Harris, B.: Theory of Probability. Addison-Wesley, 1966, pp. 191-196.

23. Landau, L. D.: On the Energy Loss of Fast Particles by Ionization. J. Phys. USSR 8, 1944, pp. 201-205.

24. Vavilov, P. V.: Ionization Losses of High-Energy Heavy Particles. JETP 5, 1957, pp. 749-751.

25. Watts, J. W.: Calculation of Energy Deposition Distributions for Simple Geometries. NASA TN D-7195, 1973.

26. Caldwell, J. H.: Charge Composition and Energy Spectra of Cosmic-Ray Nuclei at Energies Above 5 GeV per Nucleon. Astrophysical Journal, Vol. 218, 1977, pp. 269-285.

27. Janni, J. F.: Calculations of Energy Loss, Range, Pathlength, Straggling, Multiple Scattering, and the Probability of Inelastic Nuclear Collisions for 0.1- to 1000-MeV Protons. Air ForcesWeapons Lab. Report AFWL-TR-65-150, Kirtland Air Force Base, N. Mexico, 1966.

28. Sternheimer, R. M.: The Density Effect for the Ionization Loss in Various Materials. Physical Review, Vol. 88, No. 4, 1952, pp. 851-859.

29. Watts, J. W.: High Energy Physics Branch, Astrophysics Division, Space Science Lab., Huntsville, AL, personal communication, 1983.

BIBLIOGRAPHY

Aitchison, J. and Brown, J. A.: The Lognormal Distribution. Cambridge Univ. Press, 1963.

Fichtel, C. E. and Trombka, J. I.: Gamma Ray Astrophysics. NASA SP-453, 1981.

Longair, M. S. and Warner, J. W.: Scientific Research With the Space Telescope. NASA CP-2111, IAU Colloquium No. 54, August 1979.

Neyman, J. and Scott, E. L.: Processes of Clustering and Applications in Stochastic Point Processes: Statistical Analysis, Theory, and Applications. P. A. W. Lewis (ed.), Wiley-Interscience, New York, 1972, pp. 646-681.

Oegelman, H. and Wayland, J. R. (ed. by): Introduction to Experimental Techniques of High-Energy Astrophysics. NASA SP-243, 1970.

Rossi, B.: Cosmic Rays. McGraw-Hill, Inc., 1964.

Sandstroem, A. E.: Cosmic Ray Physics. North-Holland Publishing Co., Amsterdam, 1965.

Srinivasan, S. K.: Stochastic Theory and Cascade Processes. Amer. Elsevier Pub. Co., Inc., New York 1969.

Thomas, M.: A Generalization of Poisson's Binomial Limit for Use in Ecology. Biometrika 36, Vol. 18, 1949.

1. REPORT NO.	2. GOVERNMENT ACCESSION NO.	3. RECIPIENT'S CATALOG NO.
NASA TP-2337		

4. TITLE AND SUBTITLE	5. REPORT DATE
A Stochastic Model for Photon Noise Induced by Charged Particles in Multiplier Phototubes of the Space Telescope Fine Guidance Sensors	June 1984
	6. PERFORMING ORGANIZATION CODE
7. AUTHOR(S)	8. PERFORMING ORGANIZATION REPORT #
Leonard W. Howell and Hans F. Kennel	
9. PERFORMING ORGANIZATION NAME AND ADDRESS	10. WORK UNIT NO.
George C. Marshall Space Flight Center Marshall Space Flight Center, Alabama 35812	M-454
	11. CONTRACT OR GRANT NO.
	13. TYPE OF REPORT & PERIOD COVERED
12. SPONSORING AGENCY NAME AND ADDRESS	Technical Paper
National Aeronautics and Space Administration Washington, D.C. 20546	14. SPONSORING AGENCY CODE

15. SUPPLEMENTARY NOTES

Prepared by Systems Dynamics Laboratory, Science and Engineering.

16. ABSTRACT

The Space Telescope (ST) will be subjected to charged particle strikes in its space environment. ST's onboard Fine Guidance Sensors utilize multiplier phototubes (PMT) for attitude determination. These tubes, when subjected to charged particle strikes, generate "spurious" photons in the form of Cerenkov radiation and fluorescence which give rise to unwanted disturbances in the pointing of the telescope.

This paper presents a stochastic model for the number of these spurious photons which strike the photocathode of the multiplier phototube which in turn produce the unwanted photon noise. The model is applicable to both galactic cosmic rays and charged particles trapped in the Earth's radiation belts.

The model which has been programmed allows for easy adaption to a wide range of particles and different parameters for the phototube of the multiplier.

The probability density functions for photon noise caused by protons, alpha particles, and carbon nuclei were generated using thousands of simulated strikes. These distributions will be used as part of an overall ST dynamics simulation.

The sensitivity of the density function to changes in the window parameters has also been investigated.

17. KEY WORDS	18. DISTRIBUTION STATEMENT
Cerenkov radiation, cosmic ray, multiplier phototube, photon noise, random number, simulation, space telescope, attitude control	STAR Category: 73 Unclassified—Unlimited

19. SECURITY CLASSIF. (of this report)	20. SECURITY CLASSIF. (of this page)	21. NO. OF PAGES	22. PRICE
Unclassified	Unclassified	67	A04

For sale by National Technical Information Service, Springfield, Virginia 22161

NASA-Langley, 1984

LIBRARY MATERIAL SLIP

DO NOT REMOVE SLIP FROM MATERIAL

Delete your name from this slip when returning material to the library.

NAME	DATE	MS
BLY, J	7/25/00	231

NASA Langley Form 474 (Rev. Oct. 1999)